

1 **HPF1-dependent histone ADP-ribosylation triggers chromatin relaxation to promote**
2 **the recruitment of repair factors at sites of DNA damage**

3

4 Rebecca Smith^{1,†,*}, Siham Zentout^{1,†}, Catherine Chapuis¹, Gyula Timinszky^{2,*} and Sébastien
5 Huet^{1,3,*}

6 1 Univ Rennes, CNRS, IGDR (Institut de génétique et développement de Rennes) - UMR
7 6290, BIOSIT – UMS3480, F- 35000 Rennes, France

8 2 Lendület Laboratory of DNA Damage and Nuclear Dynamics, Institute of Genetics,
9 Biological Research Centre, Eötvös Loránd Research Network (ELKH), 6276 Szeged,
10 Hungary

11 3 Institut Universitaire de France, F-75000 Paris, France

12 † These authors contributed equally to this work

13 *Correspondence to: R.S. (rebecca.smith@univ-rennes1.fr), G.T. (timinszky.gyula@brc.hu),
14 or S.H. (sebastien.huet@univ-rennes1.fr)

15

16

17 **ABSTRACT**

18

19 PARP1 activity is regulated by its cofactor HPF1. The binding of HPF1 on PARP1 controls
20 the grafting of ADP-ribose moieties on serine residues of proteins nearby the DNA lesions,
21 mainly PARP1 and histones. However, the impact of HPF1 on DNA repair regulated by
22 PARP1 remains unclear. Here, we show that HPF1 controls both the number and the length
23 of the ADP-ribose chains generated by PARP1 at DNA lesions. We demonstrate that HPF1-
24 dependent histone ADP-ribosylation, rather than auto-modification of PARP1, triggers the
25 rapid unfolding of the chromatin structure at the DNA damage sites and promotes the
26 recruitment of the repair factors CHD4 and CHD7. Together with the observation that HPF1
27 contributes to efficient repair both by homologous recombination and non-homologous end
28 joining, our findings highlight the key roles played by this PARP1 cofactor at early stages of
29 the DNA damage response.

30

31 **INTRODUCTION**

32

33 Poly(ADP-ribose) Polymerase 1 (PARP1), which belongs to the diphtheria toxin-like
34 family of ADP-ribosyltransferases, is the founding member of a large family of enzymes that
35 regulate a number of different cellular processes. PARP1 itself plays pivotal functions in

36 DNA repair, chromatin folding and gene transcription^{1,2}. As part of its role in the DNA
37 damage response (DDR), PARP1 detects both single and double strand breaks³ through its N-
38 terminal DNA-binding domain consisting of three zinc fingers modules⁴. The binding of this
39 domain to DNA breaks triggers the catalytic activity of the C-terminal domain via a complex
40 allosteric mechanism⁵. Once activated, PARP1 utilizes NAD⁺ to polymerize ADP-ribose
41 (ADPr) chains on target proteins, with the major targets being histones and PARP1 itself^{6,7}.

42 Early research into PARP1 focused on its role as a discrete enzyme, capable of
43 catalyzing the addition of ADP-ribose chains alone. However, recent studies identified a key
44 co-factor, Histone Poly(ADP-ribosylation) Factor 1 (HPF1), which is required for targeting
45 ADPr chains on specific residues⁸. Indeed, HPF1 binding to the C-terminus of PARP1 creates
46 a joint catalytic site that is essential to ADP-ribosylate serines⁹, which are the main residues to
47 be modified by ADPr in the context of the DDR¹⁰. The loss of HPF1 therefore has several
48 effects; firstly, auto-modification of PARP1 shifts from occurring on serines to primarily to
49 glutamic and aspartic acids and secondly, trans ADP-ribosylation of histones is suppressed¹¹.
50 Moreover, *in vitro*, HPF1 is not only required for targeting ADPr to specific residues, but it
51 also controls the rate of polymerization, favoring mono-ADPr modifications over poly-ADPr
52 chains¹²

53 The major findings reported over the last years have allowed to considerably improve
54 our understanding of the molecular mechanisms underlying the control of ADP-ribosylation
55 signaling by the PARP1/HPF1 axis. Nevertheless, the exact impact of HPF1 on cellular
56 functions known to be regulated by PARP1 remains unclear. A role for HPF1 in DNA repair
57 has been hinted at as HPF1-deficiency led to cell hypersensitivity to DNA-damaging agents⁸.
58 Therefore, in this report, we aimed to further investigate how HPF1 could regulate ADP-
59 ribosylation-dependent steps of the DDR. We show that HPF1 is recruited to DNA lesions
60 via its binding to the C-terminal residues of PARP1 and that it controls both the number and
61 length of ADPr chains at sites of damage. We also establish that HPF1-dependent histone
62 ADP-ribosylation, rather than PARP1 auto-modification, is a major trigger of the early
63 chromatin unfolding that occurs in the vicinity of the DNA lesions, thus facilitating the
64 recruitment of subsequent repair factors. Therefore, we demonstrate that HPF1 is a central
65 player at early stages of the DDR and that its role in the regulation of chromatin structure
66 contributes to efficient DNA repair.

67

68 RESULTS

69

70 **HPF1 recruitment to sites of DNA damage relies on interaction with the C-terminus of**
71 **PARP1**

72

73 HPF1 interacts with the C-terminal end of PARP1, the last two residues L1013/W1014
74 of the latter being essential for this interaction^{9,13}. Nevertheless, the contribution of this
75 interaction to the rapid recruitment of HPF1 at DNA lesions⁸ remains unclear since recent
76 findings suggest that HPF1 and PARP accumulate to sites of damage independently from
77 each other¹⁴. To investigate this question further, we first quantified the recruitment of both
78 HPF1 and PARP1 to sites of damage induced by laser-microirradiation in U2OS *PARP1*^{KO}
79 cells co-expressing mCherry-PARP1 and GFP-HPF1 (Figure 1A,B). While the recruitment of
80 both proteins peaked within 10 sec, we observed that PARP1 accumulation to sites of damage
81 was much stronger than HPF1. This difference in the relative amounts of the two proteins
82 accumulating at DNA lesions is in line with the *in vitro* data suggesting that HPF1 can exert
83 its regulatory role on PARP1 even at low relative molarity¹⁵. Interestingly, HPF1 dissipated
84 from the damage slower than PARP1 (Fig 1C), indicating that the HPF1/PARP1 molarity
85 ratio increases progressively at DNA lesions during the first 10 minutes following damage
86 induction.

87 In agreement with previous results⁸, we found that PARP1 deficiency nearly fully
88 suppressed HPF1 recruitment to DNA lesions, the presence of PARP2 being unable to
89 compensate for PARP1 loss despite the known interaction between HPF1 and PARP2 (Fig
90 1D and Fig S1A). HPF1 recruitment in *PARP1*^{KO} cells was rescued upon re-expression of a
91 wild-type version of PARP1 (PARP1-WT) but not in the presence of PARP1 mutated at
92 residues L1013A/W1014A (PARP1-LW/AA) (Fig 1D). These data indicate that the
93 interaction of HPF1 with these last two PARP1 residues is critical for HPF1 accumulation to
94 sites of damage. We also observed that PARP1 tagged at its C-terminal end is unable to
95 rescue HPF1 recruitment when expressed in *PARP1*^{KO} cells, therefore, this tagging strategy
96 should be avoided when assessing PARP1 behavior at sites of damage (Fig S1B).

97 Beside its recruitment to sites of damage, we also wondered whether HPF1 release
98 could be regulated by the mobilization of PARP1 from this area. Auto-ADP-ribosylation of
99 PARP1 is a key regulator of its release from the DNA lesions¹⁶. Therefore, we analyzed
100 HPF1 release in *PARP1*^{KO} cells re-expressing PARP1 mutants displaying impaired auto-
101 ADP-ribosylation (Fig S1B,C) due to either suppressed catalytic activity (PARP1 E988K) or
102 mutations of the main serine residues targeted for ADP-ribosylation on PARP1 (PARP1-
103 S499/507/519A, PARP1-3SA). As previously shown¹⁶⁻¹⁸, both mutants were retained longer
104 at sites of damage compared to PARP1-WT and we observed that HPF1 release kinetics

105 mirrored the relative dissipation speeds of the different PARP1 mutants (Fig 1E-G). These
106 findings highlight that the transient accumulation of HPF1 at damage sites is tightly
107 controlled by PARP1 during both the accumulation and the release phases.

108

109 **HPF1 controls the number and length of ADP-ribose chains at sites of damage**

110

111 HPF1 controls both the targeting of ADP-ribose (ADPr) chains on specific residues and the
112 rate of ADP-ribosylation^{11,15}. Therefore, we wondered what the overall impact of the loss of
113 HPF1 on ADP-ribosylation signaling was at sites of damage by analyzing the recruitment
114 kinetics of two different ADPr-binding domains. Firstly, the macrodomain of macroH2A1.1,
115 which associates with mono-ADPr or the terminal residue of poly-ADPr chains (^{19,20}, Fig
116 2A), was used as a proxy for the number of ADPr chains at sites of damage. Secondly, the
117 WWE domain of RNF146, which binds at the interface between two monomers along poly-
118 ADPr chains, was used to estimate the total amount of ADPr (²¹, Fig 2A). Both ADPr-binding
119 domains showed similar behavior upon laser irradiation: an initial peak of recruitment within
120 the first 30 s post damage followed by a stable or slowly decreasing plateau within the next
121 10 minutes (Fig 2B-E). These recruitment profiles suggest that ADP-ribosylation signaling
122 starts with an early acute phase followed by a more sustained period lasting for several
123 minutes after damage. Importantly, this sustained signaling period arises from a dynamic
124 equilibrium between ADP-ribose polymerase and hydrolase activities since the acute
125 inhibition of PARP1 during this period leads to the rapid removal of the ADPr chains from
126 the sites of damage²².

127 We found that HPF1 deficiency was associated with a strong reduction in macrodomain
128 recruitment (Fig 2B,C). Similar defect was also observed in *PARP1*^{KO} cells expressing
129 PARP1-LW/AA, which is unable to recruit HPF1 to DNA lesions, compared to those
130 expressing PARP1-WT (Fig S2A,C). Therefore, the absence of HPF1 at sites of damage led
131 to a decrease in the number of ADPr chains that are generated upon damage. Conversely, the
132 loss of HPF1 had no major impact on WWE accumulation to sites of damage (Fig 2D,E),
133 showing that the total amount of ADPr generated at sites of damage remained unchanged.
134 This, together with the data regarding macrodomain recruitment, suggests that the fewer
135 chains generated in the absence of HPF1 are longer. These findings agree with previous *in*
136 *vitro* results showing that HPF1 is not only crucial to initiate the grafting of ADPr chains on a
137 significant number of acceptor residues but also restrains ADPr chain length¹².

138 Recent reports have also shown that modifying the relative molarities of HPF1 and
139 PARP1 strongly impacts ADP-ribosylation activity *in vitro*^{12,15}. Therefore, we wondered

140 what the impact of the over-expression of HPF1 was, whose endogenous nuclear levels are
141 20 to 50 times lower than those of PARP1⁸, on ADP-ribosylation signaling at sites of
142 damage. HPF1 overexpression had little influence on the initial peak of both macrodomain
143 and WWE but perturbed the slower plateau phases (Fig 2F,G) with increased accumulation of
144 macrodomain while WWE was reduced at sites of damage. Therefore, the excess of HPF1
145 appears to increase the amount of ADPr chains while reducing their lengths. These data show
146 that the relative amounts of HPF1 versus PARP1 within the nucleus controls the
147 characteristics of ADP-ribosylation signaling at sites of damage.

148

149 **HPF1 is a key regulator of early chromatin relaxation at sites of DNA damage**

150

151 In addition to its role in signaling the presence of DNA lesions for repair effectors,
152 ADP-ribosylation by PARP1 also triggers rapid chromatin relaxation in the vicinity of DNA
153 breaks²³, a process that facilitates the access to the lesions²². Therefore, we wondered whether
154 HPF1 could also regulate this early chromatin remodeling process due to its regulatory role in
155 ADP-ribosylation signaling. To assess this, we monitored the amount of chromatin relaxation
156 in WT, *PARP1*^{KO}, *HPF1*^{KO} and *PARP1*^{KO}/*HPF1*^{KO} cells by a live-cell chromatin relaxation
157 assay (Fig 3A,B). In this assay, a region of chromatin is highlighted by the local
158 photoconversion of PAGFP fused to the histone H2B, which occurs simultaneously to
159 damage induction by laser irradiation at 405 nm. The changes in the level of chromatin
160 condensation at the sites of damage are estimated by measuring the thickness of the
161 photoconverted line. Chromatin relaxation at sites of damage was nearly fully suppressed in
162 the absence of PARP1. The loss of HPF1 also dramatically reduced chromatin relaxation,
163 although not to the same degree as in *PARP1*^{KO} cells. The concomitant loss of PARP1 and
164 HPF1 led to relaxation levels that were lower to those in *HPF1*^{KO} cells, showing that the
165 residual relaxation seen in these cells remains PARP1-dependent. The defect in chromatin
166 relaxation seen in *HPF1*^{KO} cells is the consequence of the absence of HPF1 at DNA lesions.
167 Indeed, the expression in *PARP1*^{KO} cells of the PARP1-LW/AA mutant or C-terminally
168 tagged PARP1, which both fail to recruit HPF1 to sites of damage, was unable to restore
169 chromatin relaxation at the level measured in cells re-expressing PARP1-WT (Fig 3C, Fig
170 S3A). Similarly, the expression of the HPF1 mutant D283A, that did not to recruit to damage
171 (Fig S3B) due to impaired interaction with PARP1^{9,13}, did not rescue chromatin relaxation in
172 *HPF1*^{KO} cells (Fig 3D).

173 Interestingly, we also found that the overexpression of wild-type HPF1 led to a
174 dramatic increase of the chromatin relaxation (Fig 3E). This massive unfolding of the

175 chromatin structure remains nevertheless reversible. Indeed, a progressive recondensation of
176 the chromatin structure was also observed in HPF1 overexpressing cells following the initial
177 relaxation phase albeit slower than for endogenous levels of HPF1. Approximately 30 min
178 post irradiation, the chromatin compaction levels were similar to those pre-damage in these
179 cells. Altogether, the findings presented in this section reveal that HPF1 plays a central role
180 in the PARP1-dependent chromatin remodeling events occurring at early stages of the DDR.

181

182 **Chromatin remodeling triggered by PARP1/HPF1 at DNA lesions does not depend on**
183 **auto ADP-ribosylation of PARP1 but rather relies on trans ADP-ribosylation of**
184 **histones**

185

186 To further investigate the mechanisms underlying the regulation of chromatin
187 remodeling by HPF1 at sites of DNA damage, we first analyzed the behaviour of the HPF1
188 mutant E284A, which still interacts with PARP1 but blocks the ADP-ribosylation activity of
189 the joined catalytic site created by the PARP1/HPF1 heterodimer⁹. While this E284A mutant
190 displayed increased recruitment to DNA lesions compared to wild-type HPF1 (Fig S3B) in
191 line with its tighter binding to PARP1¹², it was unable to rescue the chromatin relaxation
192 defect observed in *HPF1*^{KO} cells (Fig 4A). This finding demonstrates that the ADP-
193 ribosylation activity of the PARP1/HPF1 complex is needed for chromatin remodeling at
194 sites of damage.

195 Upon DNA damage, HPF1 has been shown to control the addition of ADP-ribose
196 moieties on the serine residues of specific targets¹⁰. This includes the auto ADP-ribosylation
197 of PARP1 itself but also trans ADP-ribosylation of other targets, in particular histones which
198 are the main ADP-ribosylation targets after PARP1¹⁰. Therefore, we assessed the relative
199 contributions of the ADP-ribosylation of PARP1 and the histones to the HPF1-dependent
200 chromatin relaxation observed at sites of damage. First, we found that the PARP1-3SA
201 mutant, which can still catalyze histone ADP-ribosylation due to interaction with HPF1¹⁶ but
202 shows greatly reduced auto ADP-ribosylation (Fig S1B,C), restored chromatin relaxation in
203 *PARP1*^{KO} cells similar to PARP1-WT complementation (Fig 4B). As expected, this rescue
204 relied on the presence of HPF1 since expressing PARP1-3SA in *PARP1*^{KO}/*HPF1*^{KO} cells did
205 not permit chromatin relaxation to reach the level observed in WT cells. Next, we analysed
206 the behaviour of the HPF1 mutant R239A at DNA lesions. In agreement with *in vitro*
207 observations showing that this mutation does not significantly impact the interaction with
208 PARP1¹³, we observed that HPF1-R239A was recruited to DNA lesions, although at a lower
209 level than its wild-type counterpart (Fig S4A,B). Furthermore, this mutation perturbed the

210 catalytic activity of the PARP1/HPF1 complex by preventing histone ADP-ribosylation while
211 preserving some PARP1 automodification (Fig 4C), confirming previous reports^{9,13}. When
212 expressed in *HPF1*^{KO} cells, the HPF1-R239A mutant was unable to promote chromatin
213 relaxation as observed with wild-type HPF1 complementation (Fig 4D). Together with the
214 results regarding the PARP1-3SA mutant, these findings indicate that the driving force for
215 chromatin remodelling at sites of damage is the ADP-ribosylation of histones rather than of
216 PARP1.

217 Finally, given that several chromatin remodelers were found to recruit to DNA lesions
218 and contribute to chromatin remodeling at sites of damage²³⁻²⁵, we wondered whether the
219 chromatin relaxation promoted by histone ADP-ribosylation relied on ATP-dependent
220 processes. ATP-deprivation, which leaves ADP-ribosylation signalling unaffected at sites of
221 damage²³, did not prevent the dramatic increase in chromatin relaxation observed upon
222 overexpression of HPF1 (Fig 4E). Therefore, histone ADPr appears sufficient to promote
223 chromatin unfolding, without the need for active remodeling processes.

224

225 **HPF1-dependent chromatin relaxation at DNA lesions promotes the recruitment of** 226 **repair factors**

227

228 Previous studies have indicated that ADPr-dependent chromatin remodeling contributes
229 to the efficient recruitment of several repair factors through increased accessibility to DNA at
230 sites of damage²⁴⁻²⁶. Given the central role of HPF1 in these chromatin remodeling events, we
231 investigated the impact of the loss of HPF1 on the recruitment of two repair factors, CHD4
232 and CHD7, that were both reported to accumulate at DNA lesions in response to ADPr-
233 dependent chromatin relaxation. Importantly, these two factors belong to different repair
234 pathways with CHD4 involved in homologous recombination (HR)²⁷ while CHD7
235 participates in non-homologous end-joining (NHEJ)²⁴. The accumulation of these two factors
236 to sites of damage was impaired in both *PARP1*^{KO} and *HPF1*^{KO} cells, the strength of the
237 recruitment defect mirroring the reduction in chromatin relaxation observed in both cell lines
238 (Fig 5A-D). Furthermore, expressing PARP1-3SA in *PARP1*^{KO} cells rescued the
239 accumulation of CHD4 and CHD7 to sites of damage similar to PARP1-WT
240 complementation in contrast to the expression PARP1-LW/AA in *PARP1*^{KO} or to the
241 complementation of *PARP1*^{KO}/*HPF1*^{KO} cells with PARP1-WT (Fig S5A-D). These findings
242 show that the recruitment defect observed for CHD4 and CHD7 in *HPF1*^{KO} cells is not the
243 consequence of impaired automodification of PARP1 but is rather due the reduced chromatin

244 relaxation associated with the absence of HPF1-dependent histone ADP-ribosylation at sites
245 of damage.

246 Previous data has shown that HPF1-deficient cells are hypersensitive to DNA damaging
247 agents, suggesting that DNA repair efficiency is compromised⁸. To better characterize this
248 repair defect, we depleted HPF1 in the well-established reporter cell lines DR-GFP and EJ5-
249 GFP and found that reducing HPF1 levels impaired the efficiency of DNA repair by both HR
250 and NHEJ (Fig. 5E,F and Fig. S5E-H). This result is in line with the fact that repair factors
251 involved in each of these pathways displayed reduced recruitment at DNA lesions in *HPF1*^{KO}
252 cells (Fig 5A-D).

253

254 **DISCUSSION**

255

256 ADP-ribosylation is one of the earliest signalling pathways activated during the DDR²⁸.
257 It is well-established that PARP1 is the central engine triggering this signalling pathway via
258 its rapid recruitment to DNA lesions² but recent reports have demonstrated that this process
259 also requires a steering wheel, the co-factor HPF1, to dictate the choice of the target proteins
260 that will be ADP-ribosylated⁹⁻¹¹. HPF1 was shown to associate with PARP1 to form a joint
261 catalytic site that is essential to ADP-ribosylate serine residues of target proteins such as
262 PARP1 itself or histones⁹. Nevertheless, the fact that HPF1 is much less abundant than
263 PARP1 within the cell nucleus suggests that the regulatory role played by HPF1 does not
264 require a stable association between the two partners but is rather exerted via transient
265 interaction with PARP1, which is needed to attach the first ADPr moiety on the serine
266 residues^{9,15,16}. Yet, the factors regulating this temporary association between PARP1 and
267 HPF1, and therefore, controlling HPF1 accumulation to sites of damage, remain only
268 partially described. In this report, we demonstrate that the rapid accumulation of HPF1 to
269 sites of damage fully relies on its binding to PARP1 since impairing this interaction by
270 mutating either the last two amino acids of PARP1 or the residue D283 of HPF1 suppressed
271 HPF1 recruitment to sites of damage (Fig 1, Fig S3B). We also found that, while HPF1
272 mobilization from sites of damage is influenced by the release of PARP1 (Fig 1F,G), the
273 dissipation speed of HPF1 is slower than that of PARP1 (Fig 1C) leading to a gradual
274 increase of the HPF1/PARP1 ratio at sites of damage. This finding hints for progressive
275 changes in the characteristics of ADP-ribosylation signalling along the course of the DDR.
276 While the early wave of ADP-ribosylation could be mainly composed of HPF1-independent
277 PARP1 auto-modification, trans-ADP-ribosylation of histones triggered by PARP1/HPF1
278 would arise at later stages of the DDR. Besides its role to target the residues for ADP-

279 ribosylation, HPF1 also controls the length of the ADP-ribose chains¹². Here, we show that
280 these *in vitro* data hold true in living cells and that the accumulation of HPF1 at sites of
281 damage favours the addition of ADPr chains but restricts their length (Fig 2). This damping
282 function of HPF1 is likely a central regulator of ADP-ribosylation signalling given the
283 prevalence of mono-ADPr modifications compared to poly-ADPr chains in the DDR
284 context¹¹.

285 The ADPr moieties bound to target proteins located nearby the DNA lesions are
286 recognized by multiple effectors contributing to the restoration of genomic integrity²⁹. While
287 this role as a binding platform has been studied extensively²⁹, less is known about the direct
288 impact of these ADPr chains on the function of the proteins to which they are attached to.
289 More specifically, while auto-modification of PARP1 has been shown to be important for the
290 timely mobilization of this protein from sites of damage^{16,30}, the direct impact of trans-ADP-
291 ribosylation, in particular, on histones, has not been elucidated. In this current report, we
292 demonstrate that HPF1-dependent histone ADP-ribosylation is a major contributor to the
293 transient unfolding of the chromatin in the vicinity of the DNA lesions (Fig 3,4). Seminal *in*
294 *vitro* work by Poirier and colleagues had found that the ADP-ribosylation of histones was
295 sufficient to decondense purified chromatin fibers³¹, a process that does not require histone
296 eviction^{32,33}. Our live-cell results are fully consistent with these data. Indeed, we previously
297 found that ADPr-dependent chromatin relaxation that occurs at early stages of the DDR does
298 not involve the mobilization of core histones²². Additionally, we now show that HPF1-
299 dependent histone ADP-ribosylation promotes chromatin unfolding even upon ATP-
300 deprivation, suggesting that the addition of the ADPr onto histones themselves is sufficient to
301 promote unfolding without the need for active nucleosome disassembly via chromatin
302 remodelers (Fig 4E). Also in agreement with *in vitro* results³³, the dynamic nature of ADPr,
303 which can be removed by different hydrolases such as PARG or ARH3^{29,34,35}, allows the
304 chromatin relaxation process to be fully reversible even in the context of HPF1
305 overexpression which strongly enhances this relaxation (Fig 3E). Importantly, several ATP-
306 dependent remodelers have also been shown to contribute to early chromatin relaxation at
307 sites of damage^{23-25,36}. While future work will help to define whether these two different
308 modalities of chromatin remodeling are coordinated or work independently, it was recently
309 shown that histone ADP-ribosylation can serve as a potential docking site for some
310 remodelers such as ACL1/CHD1L³⁷ known to contribute to chromatin remodeling at sites of
311 damage²³.

312 We recently proposed that the PARP-dependent chromatin relaxation observed at early
313 stages of the DDR facilitates access of DNA lesions to repair factors²². In the present work,

314 we demonstrate that this process is triggered by trans-ADP-ribosylation of histones rather
315 than auto-modification of PARP1 and that it promotes the accumulation of repair factors
316 belonging to both HR and NHEJ. The fact that HPF1 deficiency impairs the efficient of both
317 repair pathways indicates that these chromatin remodelling processes regulated by the
318 PARP1/HPF1 axis precedes the repair pathway choice and therefore are pivotal in the
319 initiation of the DDR (Fig 6).

320

321 **Acknowledgements**

322 We thank the Microscopy-Rennes Imaging Center (BIOSIT, Université Rennes 1), member
323 of the national infrastructure France-BioImaging supported by the French National Research
324 Agency (ANR-10-INBS-04), for providing access to the imaging setups, as well as S.
325 Dutertre and X. Pinson for technical assistance on the microscopes. We also thank the
326 Cytométrie en flux et tri cellulaire (BIOSIT, Université Rennes 1), specifically L. Deleurme
327 and A. Amie for technical assistance with flow cytometry. We would also like to thank I.
328 Ahel and M. Suskiewicz for thoughtful discussions and generously sharing HPF1 plasmid
329 DNA. For this work, the S.H.'s group received financial support from the Agence Nationale
330 de la Recherche (PRC-2018 REPAIRCHROM), the Institut National du Cancer (PLBIO-
331 2019) and the Institut Universitaire de France, to S.H. R.S. is supported by the Fondation
332 ARC pour la recherche sur le cancer (PDF20181208405). The work in the Timinszky
333 laboratory was supported by the Hungarian Academy of Sciences (LP2017-11/2017) and the
334 National Research Development and Innovation Office (K128239).

335

336 **Author Contributions**

337 R.S., G.T. and S.H. conceived the project with inputs from all authors. R.S., S.Z. and S.H.
338 performed live-cell imaging and analysed the imaging data. S.Z. performed the DNA repair
339 assay. C.C. and R.S. generated DNA constructs. R.S., G.T. and S.H. wrote the paper with
340 input from all authors.

341

342 **Competing interests**

343 Authors declare no competing interests.

344

345 **Methods:**

346 **Plasmids**

347 pmEGFP-WWE, PATagRFP-H2B²³, pH2B-PAGFP³⁸, pGFP-CHD4³⁹, pGFP-CHD7²⁴,
348 pPARP1-mCherry²⁰, pmCherry-PARP1 WT, pmCherry-PARP1 E988K¹⁷, pLacI-GFP trap²⁵,
349 pcDNA3.1(+) (Thermofisher) and pmCherry-C1 (Takara) were previously described.
350 pCBASceI was a gift from Maria Jasin (Addgene plasmid # 26477,⁴⁰). PARP1 3SA
351 (S499A/S507A/S519A) cDNA was amplified from pDEST-YFP-PARP1-3SA¹⁶ and ligated
352 into pmCherry-C1 between *Bg*III and *Xma*I. pmCherry-PARP1 L1013A/W1014A was made
353 using site-directed mutagenesis with primers provided in Table 1. MacroH2A1.1
354 macrodomain cDNA was amplified from pcDNA3.1-YFP-macroH2A1.1 macrodomain²⁰ and
355 ligated into pEGFP-C1 between *Bg*III and *Eco*RI. cDNA of HPF1 WT, R239A, D283A and
356 E284 were amplified from pDEST-YFP-HPF1 WT, R239A, D283A and E284⁹ with primers
357 provided in Table 1 and ligated into pEGFP-C1 or pmCherry-C1 between *Bg*III and *Bam*HI.

358

359 **Cell culture**

360 All cells used in this study were cultured in DMEM (Sigma) or RPMI supplemented with
361 10% FBS, 100 µg/mL penicillin, 100 U/mL streptomycin and maintained at 37°C in a 5%
362 CO₂ incubator. U2OS *WT*, U2OS *PARP1*^{KO}, U2OS *HPF1*^{KO}, U2OS *PARP1*^{KO} *HPF1*^{KO}
363 double knockout cells were generated previously⁸. U2OS 2B2 were generated previously⁴¹.
364 U2OS-DR and U2OS-EJ5 cells were a kind gift from Jeremy Stark⁴². All experiments
365 presented in this work were performed on unsynchronized cells.

366

367 **Live-cell microscopy**

368 U2OS cells were seeded into 8-well Imaging Chamber CG (Zell-Kontakt) and transfected 48-
369 72 h prior to imaging using XtremeGene HP (Roche) according to the manufacture's
370 instructions. Cells were sensitized by aspirating growth medium from the Lab-Tek and
371 replacing it with fresh medium containing 0.15 – 0.3 µg/mL Hoechst 33342 for 1 hour at
372 37°C. Immediately prior to imaging, growth medium was replaced with CO₂-independent
373 imaging medium (Phenol Red-free Leibovitz's L-15 medium (Life Technologies)
374 supplemented with 20% fetal bovine serum, 2 mM glutamine, 100 µg/mL penicillin and 100
375 U/mL streptomycin). ATP depletion was achieved by bathing the cells for at least 30 min
376 with PBS containing 10% fetal bovine serum, 10 mM NaN₃ and 50 mM 2-deoxyglucose
377 (Platani et al., 2002). Live-cell imaging experiments were completed on a Ti-E inverted
378 microscope from Nikon equipped with a CSU-X1 spinning-disk head from Yokogawa, a Plan
379 APO 60x/1.4 N.A. oil-immersion objective lens and a sCMOS ORCA Flash 4.0 camera. The
380 fluorescence of EGFP/PAGFP and mCherry/PATagRFP were excited with lasers at 490 and
381 561 nm, respectively. For fluorescence detection, we used bandpass filters adapted to the

382 fluorophore emission spectra. Laser microirradiation and local photoactivation at 405 nm was
383 performed along a 16 μm -line through the nucleus using a single-point scanning head (iLas2
384 from Roper Scientific) coupled to the epifluorescence backboard of the microscope. To
385 ensure reproducibility laser power at 405 nm was measured at the beginning of each
386 experiment and set to 125 μW at the sample level. Cells were maintained at 37°C with a
387 heating chamber. Protein recruitment was quantified using a custom-made MATLAB
388 (MathWorks) routine which measures the mean intensity within the damaged region (I_d) as
389 determined by the segmentation of the photoactivated H2B signal, the mean nuclear
390 fluorescence (I_{nd}), and the mean background signal outside of the cell (I_{bg}). Protein
391 accumulation at sites of damage (A_d) was then calculated as:

$$A_d = \frac{I_d - I_{bg}}{I_n - I_{bg}}$$

394
395 The intensity within the microirradiated area was then normalized to the intensity prior to
396 damage induction.

397 Chromatin relaxation was determined using a custom MATLAB routine that measures the
398 changes in the thickness of the photoconverted H2B line relative to its value immediately
399 after damage induction²³.

400 The PAR3H assay has been previously described²⁵. Briefly, U2OS-2B2⁴¹ cells containing the
401 LacO array were transfected with GFP-macrodomein of macroH2A1.1, LacI-GFP trap and
402 mCherry-PARP1, mCherry-PARP1 E988K or mCherry-PARP1 3SA. Cells sensitized with
403 Hoechst 33342 were irradiated away from the LacO array with 405 nm light to induce DNA
404 damage as described above. No matter whether it is ADP-ribosylation status, PARP1 does
405 not remain stably bound to DNA lesions but can quickly dissociate from this region and
406 diffuse within the nucleus^{17,18}. Therefore, the amount of accumulation of mCherry tagged
407 PARP1 at the LacO array due to interaction with tethered macrodomain can then be used as a
408 proxy to assess the level of ADP-ribosylation of the different PARP1 mutants. The mCherry
409 intensity at the LacO array (A_{lo}) quantified with the following equation where I_o is the
410 intensity of the LacO array, I_n is the mCherry signal in the nucleoplasm devoid of the LacO
411 array and I_{bg} is the intensity of the background:

$$A_{lo} = \frac{I_o - I_{bg}}{I_n - I_{bg}}$$

413

414 The intensity within the LacO array was then normalized to the intensity prior to damage
415 induction.

416

417 **DNA repair assay**

418 U2OS-DR and U2OS-EJ5 cells containing either a stably integrated cassette of the DR-GFP
419 or EJ5-GFP reporter were used to measure the repair of I-SceI-induced DSBs by homologous
420 recombination or by non-homologous end joining, respectively⁴². Briefly, cells were
421 transfected with siRNA for 48 h prior to co-transfected with an mCherry expression vector
422 and the I-SceI expression vector. The percentage of GFP-positive cells among the mCherry-
423 positive cells was determined 48 h after I-SceI transfection using a LSRFortessa X-20 (BD
424 Bioscience) using BD FACSDiva Software v8.0.1. Quantifications were performed with
425 FACSDiva™ (BD Biosciences). siRNAs used in this study are shown in Table 2.

426

427 **Western Blotting**

428 For whole cell extract, cells were lysed on with Triton-X buffer (% Triton X-100, 100 mM
429 NaCl and 50 mM Tris-HCl, pH 8.0, 5 mM MgCl₂, 0.1% Benzonase (Sigma Aldrich), 1x
430 protease inhibitor (Roche) on an orbital rotator at 4°C for 30 min. Samples were centrifuged
431 at 20 000 g for 15 min and supernatant was collected. Protein samples were quantified using
432 Bradford (BioRad) and equal amounts of protein were loaded on gels for SDS-PAGE prior to
433 immunoblotting. Antibodies used in this study are given in Table 3. For DNA damage
434 induction, cells were incubated in serum free media prior to treatment with 2 mM H₂O₂ for
435 10 min. During cell lysis, Triton-X buffer was supplemented further with 2 μM olaparib
436 (Selleckchem) and 2 μM PARG inhibitor PDD00017273 (Sigma Aldrich)

437

438 **Statistics**

439 Data analysis and visualization was performed using R software (<https://www.r-project.org/>).
440 The boxplot limits correspond to the 25th and 75th percentiles and the bold line indicates the
441 median value. The whiskers extend 1.5 times the interquartile range. The timelapse curves are
442 the mean ± SEM of at least 15 cells per condition from a characteristic experiment among at
443 least three independent repeats. The histograms show the mean ± SEM of the indicated
444 independent experiments number in the figure legends. Unless stated otherwise, p values
445 were calculated using an unpaired Student's t test, assuming unequal variances.

446

447 **Table 1:** List of primers used in this study

Name	Sequence (5'-3')
MacroH2A1.1 macrodomain For	GGAGATCTCAGGGTGAAGTCAGTAA
MacroH2A1.1 macrodomain Rev	CCGGAATTCCTAGTTGGCGTCCAGCTT
PARP1-L1013A/W1014A For	GAAATTCAATTTTAAGACCTCCGCGGCGTAACCCGGGAT CCACCGGATC
PARP1-L1013A/W1014A Rev	GATCCGGTGGATCCCGGGTTACGCCGCGGAGGTCTTAAA ATTGAATTTC
mCherry-C1-PARP1 For	ATATAGATCTATGGCGGAGTCTTCGG
mCherry-C1-PARP1 Rev	ATACCCGGGTTACCACAGGGAGGTC
pmCherry/pEGFP-C1 HPF1 For	ATATAGATCTATGGTTCGGCGGTGG
pmCherry/pEGFP-C1 HPF1 Rev	ATATGGATCCTCATGCAGCAAGTTGG

448

449 **Table 2:** List of siRNA used in this study

Target	Reference/ sequence	Company
siCTRL	4390843	Ambion Silencer Select
siBRCA2	S2083	Ambion Silencer Select
siHPF1_1	S29881	Ambion Silencer Select
siHPF1_2	S29882	Ambion Silencer Select
siXRCC4	AUAUGUUGGUGAACUGAGA	Eurogentec

450

451 **Table 3:** List of antibodies used in this study

Target	Host	Company	Reference	Dilution in WB
Primary Antibodies				
PARP1	Rabbit	-	Sellou et al. ²³	1:10000
PARP2	Rabbit	Active Motif	#39744	1:1000
HPF1	Rabbit	Novus Biologicals	NBP1-93973	1:500
Actin	Mouse	Sigma	A5060	1:1000
XRCC4	Mouse	Abcam	Ab213729	1:500
BRCA2	Rabbit	Novus Biologicals	MAB2476	1:500
RFP/mCherry	Mouse	Chromotek	6g6-100	1:1000

H3	Rabbit	Abcam	Ab1731	1:2500
PAN- ADPr binding reagent	Rabbit	Sigma	MABE1016	1:1500
Secondary Antibodies				
Anti-Mouse-HRP	Goat	Agilent	P044701-2	1:3000
Anti-Rabbit-HRP	Swine	Agilent	P039901-2	1:3000-1:8000

452

453

454 **Figure Legends**

455

456 **Figure 1: HPF1 recruitment to sites of damage relies on interaction with the C-terminus**

457 **of PARP1.** (A) Representative images of mCherry-PARP1 and GFP-HPF1 recruitment to
 458 sites of DNA damage induced by laser irradiation, in *PARP1^{KO}* cells. Scale bar, 5 μ m. (B)
 459 Recruitment kinetics of mCherry-PARP1 (black) and GFP-HPF1 (red) to sites of DNA
 460 damage. (C) To assess the relative release kinetics of mCherry-PARP1 and GFP-HPF1, the
 461 time $t_{1/2}$ at which half of PARP1-WT has been released compared to peak accumulation was
 462 first estimated from the mean curve shown in B. Then, the amount of the different proteins is
 463 measured at $t_{1/2}$ for each individual cell and normalized to peak accumulation to estimate the
 464 relative residual accumulation. (D) Recruitment kinetics of GFP-HPF1 to sites of DNA
 465 damage in *WT* or *PARP1^{KO}* cells expressing mCherry-tagged PARP1 WT or PARP1
 466 L1013A/W1014A (PARP1-LW/AA). (E, F) Recruitment kinetics of (E) mCherry-PARP1-
 467 3SA (black) or (F) mCherry-PARP1-E988K (black) and GFP-HPF1 (red) to sites of DNA
 468 damage. (G) With the same approach as for panel C, the relative residual accumulation of
 469 mCherry tagged PARP1 mutants and GFP-HPF1 was estimated from the curves shown in E
 470 and F.

471

472 **Figure 2: HPF1 regulates ADP-ribosylation signalling at sites of DNA damage.** (A)

473 Schematic representation of WWE and macrodomain recruitment on ADPr chains. (B)
 474 Representative images showing recruitment of the macrodomain of macroH2A1.1 to sites of
 475 DNA damage induced by laser irradiation in *WT* and *HPF1^{KO}* cells. Scale bar, 5 μ m. (C)
 476 Recruitment kinetics of the macrodomain to sites of DNA damage in *WT* (black) and *HPF1^{KO}*
 477 (red) cells. (D) Representative images showing recruitment of the WWE domain of RNF146
 478 to sites of laser induced DNA damage in *WT* and *HPF1^{KO}* cells. Scale bar, 5 μ m. (E)
 479 Recruitment kinetics of the WWE domain to sites of DNA damage in *WT* (black) and
 480 *HPF1^{KO}* (red) cells. (F, G) Recruitment kinetics of (F) GFP-WWE or (G) GFP-macrodomain

481 of mH2A1.1 recruitment kinetics at sites of DNA damage in U2OS *WT* cells overexpressing
482 mCherry-HPF1 or not. Data are shown as mean \pm SEM.

483

484 **Figure 3: HPF1 promotes chromatin relaxation at sites of DNA damage.** (A) Left:

485 Confocal image sequences of the chromatin line area which got simultaneously damaged and

486 photoconverted by irradiation at 405 nm in U2OS *WT*, *PARP1^{KO}*, *HPF1^{KO}* and *PARP1/HPF1*

487 double knockout cells expressing H2B-PAGFP. Scale bars, 2 μ m. Right: Intensity profiles

488 perpendicular to the irradiated lines (μ m) at 0 s (black) and 120 s (red) after damage

489 induction. The enlargement of the profile is due to the thickening of the photoconverted line

490 consecutive to chromatin relaxation (B) Chromatin relaxation in U2OS *WT*, *PARP1^{KO}*,

491 *HPF1^{KO}* and *PARP1/HPF1* double knockout cells, assessed by the thickness of the

492 highlighted damaged chromatin line at 120 s relative to 0 s post irradiation. (C) Chromatin

493 relaxation at 120 s post irradiation in *WT* and *PARP1^{KO}* cells expressing mCherry-PARP1

494 WT or PARP1-LW/AA. \emptyset denotes no plasmid expression. (D) Chromatin relaxation at 120 s

495 post-irradiation in *WT* and *HPF1^{KO}* cells expressing mCherry-HPF1 D283A. \emptyset denotes no

496 plasmid expression. (E) Kinetics of chromatin relaxation in U2OS *WT* cells overexpressing

497 or not mCherry-HPF1. Data are shown as mean \pm SEM.

498

499 **Figure 4: HPF1-dependent chromatin relaxation relies on trans ADP-ribosylation of**

500 **histones rather than PARP1 auto-modification** (A) Chromatin relaxation at 120 s post-

501 irradiation in *WT* and *HPF1^{KO}* cells expressing or not mCherry-HPF1 E284A. \emptyset denotes no

502 plasmid expression. (B) Chromatin relaxation at 120s post-irradiation in U2OS *WT*,

503 *PARP1^{KO}*, *HPF1^{KO}* and *PARP1/HPF1* double knockout cell. Cells are complemented either

504 with mCherry-PARP1 WT or with PARP1-3SA mutant. \emptyset denotes no plasmid expression.

505 (C) Western blot displaying ADPr signals, stained with a pan-ADPr antibody, in *WT* and

506 *HPF1^{KO}* cells expressing HPF1-WT or HPF1-R239A and treated or not with H₂O₂. H3 and

507 Tubulin were used as loading controls. (D) Chromatin relaxation at 120 s post-irradiation in

508 *WT* and *HPF1^{KO}* cells expressing mCherry-HPF1 R239A. \emptyset denotes no plasmid expression.

509 (E) Chromatin relaxation at 120 s post-irradiation in U2OS *WT* cells overexpressing

510 mCherry-HPF1 and depleted or not for ATP (ATPi). \emptyset denotes no plasmid expression.

511

512 **Figure 5: HPF1-dependent chromatin relaxation promotes the recruitment of both**

513 **homologous recombination and non-homologous end joining repair factors.** (A)

514 Representative confocal images showing recruitment of GFP-CHD4 to sites DNA damage

515 induced by laser irradiation, in U2OS *WT*, *HPF1^{KO}* or *PARP1^{KO}* cells. Scale bar, 5 μ m. **(B)**
516 Recruitment kinetics of GFP-CHD4 to sites of DNA damage in U2OS *WT*, *HPF1^{KO}* or
517 *PARP1^{KO}* cells. **(C)** Representative confocal images showing recruitment of GFP-CHD7 to
518 sites of DNA damage induced by laser irradiation, in U2OS *WT*, *HPF1^{KO}* or *PARP1^{KO}* cells.
519 Scale bar, 5 μ m. **(D)** Recruitment kinetics of GFP-CHD7 to sites of DNA damage in U2OS
520 *WT*, *HPF1^{KO}* or *PARP1^{KO}* cells. **(E)** Quantification of DR-GFP-positive U2OS cells
521 transfected with the indicated siRNA and I-SceI expression vector. The mean \pm SEM of 5
522 independent experiments is shown. Data were normalized to siCTRL, which was set to 100%.
523 **(F)** Quantification of EJ5-GFP-positive U2OS cells transfected with the indicated siRNA and
524 I-SceI expression vector. The mean \pm SEM of 6 independent experiments is shown. Data
525 were normalized to siCTRL, which was set to 100%.

526

527 **Figure 6: HPF1 regulates DNA damage induced chromatin relaxation.** Upon damage,
528 HPF1 interacts with PARP1 at sites of damage and promote both PARP1 auto-modification
529 and trans ADP-ribosylation of histone. Histone ADP-ribosylation promotes chromatin
530 relaxation in the vicinity of DNA lesions, promoting the recruitment of repair factors to
531 facilitate genome restoration by both homologous recombination and non-homologous end
532 joining.

533

534

535 **Supplementary figure legends:**

536

537 **Supp Figure 1: HPF1 recruitment to sites of damage relies on interaction with the C-**
538 **terminus of PARP1** **(A)** Immunoblots of whole cell extract from U2OS *WT*, *PARP1^{KO}*,
539 *HPF1^{KO}* and *PARP1/HPF1* double knockout cells. Actin is used as a loading control. **(B)**
540 Recruitment kinetics of GFP-HPF1 to sites of DNA damage in *WT* or *PARP1^{KO}* cells
541 expressing WT N-terminally (mCh-PARP1) and C-terminally tagged PARP1 (PARP1-mCh).
542 Data are shown as mean \pm SEM. **(C)** Schematic representation of PAR-3H assay. In this
543 assay, mCherry-tagged PARP1 variants are expressed together with the GFP-tagged
544 macrodomain of macroH2A1.1, that is tethered to a LacO array integrated into the genome of
545 U2OS 2B2 cells. Upon laser irradiation, the PARP1 variants recruit to sites of damage, where
546 they can be auto ADP-ribosylated or not, depending on the variant. A defect in auto ADP-
547 ribosylation does not preclude high turnover at sites of damage, allowing all PARP1 variants
548 to diffuse rapidly within the nucleus after their release from the DNA lesions. If PARP1 is
549 ADP-ribosylated it can then interact with the tethered macrodomain leading to an increase in

550 mCherry signal at the LacO array. **(D)** Representative confocal images of PARP1-WT,
551 PARP1-3SA or PARP1-E988K to YFP-macrodomain of mH2A1.1 tethered to LacO. Inset,
552 pseudocolored according to the look-up table displayed, shows the magnified LacO array.
553 Post-irradiation images are shown at 30 seconds. Scale bar, 5 μ m. **(E)** Quantification of the
554 accumulation of PARP1-WT, PARP1-3SA or PARP1-E988K to the LacO array after DNA
555 induction by laser irradiation.

556

557 **Supp Figure 2: HPF1 regulates ADP-ribosylation signalling at sites of DNA damage.**

558 **(A)** Recruitment kinetics of GFP-macrodomain of mH2A1.1 at sites of DNA damage induced
559 by laser irradiation, in U2OS *PARP1*^{KO} cells complemented or not with mCherry-PARP1
560 WT, PARP1-3SA or PARP1-LW/AA. **(B)** Quantification of mean intensity of GFP-
561 macrodomain of mH2A1.1 at sites of DNA damage 200 s post-irradiation in *PARP1*^{KO}
562 complemented or not with mCherry-PARP1 WT or PARP1-LW/AA mutants. \emptyset denotes no
563 plasmid expression.

564

565 **Supp Figure 3: HPF1 promotes chromatin relaxation at sites of DNA damage (A)**

566 Chromatin relaxation in U2OS *WT* or *PARP1*^{KO} cells at 120 s post-irradiation. Cells are
567 complemented or not with C-terminally-tagged PARP1-mCherry. \emptyset denotes no plasmid
568 expression. **(B)** Recruitment kinetics of mCherry-tagged HPF1 WT and the point mutants
569 D283A and E284A at sites of DNA damage in U2OS *HPF1*^{KO} cells.

570

571 **Supp Figure 4: HPF1-dependent chromatin relaxation relies on trans ADP-ribosylation
572 of histones rather than PARP1 auto-modification (A)**

573 Representative images of the
574 recruitment of mCherry-tagged HPF1 WT or HPF1-R239A to sites DNA damage induced by
575 laser irradiation in U2OS *HPF1*^{KO} cells. Scale bar, 5 μ m. **(B)** Recruitment kinetics of
576 mCherry-tagged HPF1 WT or HPF1-R239A mutant at sites of DNA damage in U2OS
577 *HPF1*^{KO} cells.

577

578 **Supp Figure 5: HPF1 contributes to efficient repair by homologous recombination and
579 non-homologous end joining. (A)**

580 Recruitment kinetics of GFP-CHD4 to sites DNA damage
581 in U2OS *WT*, *HPF1*^{KO} or *PARP1*^{KO} complemented or not with PARP1 WT or PARP1-3SA.

582 **(B)** Quantification of mean intensity of GFP-CHD4 at sites DNA damage 200 s post-
583 irradiation, in *PARP1*^{KO} or *PARP1/HPF1* double knockout cells complemented or not with
584 mCherry-PARP1 WT, PARP-3SA or PARP1-LW/AA mutants. \emptyset denotes no plasmid

584 expression. (C) Recruitment kinetics of GFP-CHD7 to sites of DNA damage in U2OS *WT*,
585 *HPF1^{KO}* or *PARP1^{KO}* complemented or not with PARP1 WT or PARP1-3SA. (D)
586 Quantification of mean intensity of GFP-CHD7 at sites of DNA damage 200 s post-
587 irradiation, in *PARP1^{KO}* or *PARP1/HPF1* double knockout cells complemented or not with
588 mCherry-PARP1 WT, PARP-3SA or PARP1-LW/AA mutants. ∅ denotes no plasmid
589 expression. (E) Schematic representation of the HR reporter assay (DR). After cleavage with
590 I-SceI, the double-strand-breaks repaired by HR results in GFP expression. (F)
591 Representative immunoblots showing the knockdown of BRCA2 and HPF1 in DR cells.
592 Actin is used as a loading control. (G) Schematic representation of the NHEJ reporter assay
593 (EJ5). Double cleavage by I-SceI removes the Puro cassette and the repair of the double-
594 strand-break by NHEJ allows GFP expression. (H) Representative immunoblots showing
595 knockdown of XRCC4 and HPF1 in EJ5 cells. Actin is used as a loading control.

596
597

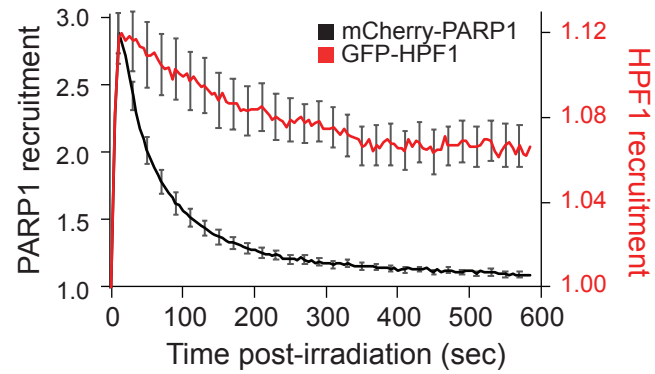
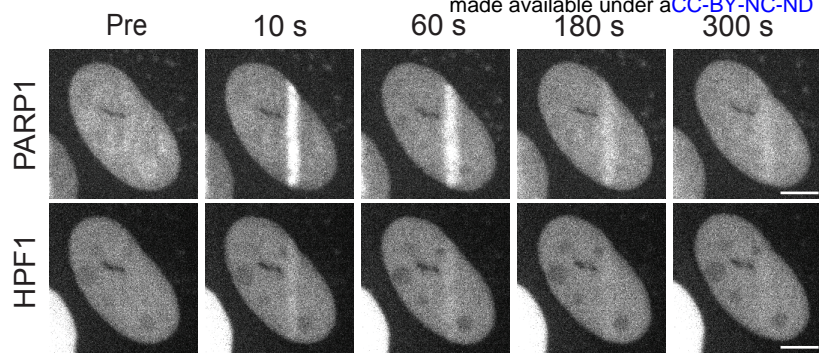
598 References

- 599 1. Kraus, W.L. & Hottiger, M.O. PARP-1 and gene regulation: progress and puzzles.
600 *Mol Aspects Med* **34**, 1109-23 (2013).
- 601 2. Ray Chaudhuri, A. & Nussenzweig, A. The multifaceted roles of PARP1 in DNA
602 repair and chromatin remodelling. *Nat Rev Mol Cell Biol* (2017).
- 603 3. Eustermann, S. et al. Structural Basis of Detection and Signaling of DNA Single-
604 Strand Breaks by Human PARP-1. *Mol Cell* **60**, 742-754 (2015).
- 605 4. Ali, A.A.E. et al. The zinc-finger domains of PARP1 cooperate to recognize DNA
606 strand breaks. *Nat Struct Mol Biol* **19**, 685-692 (2012).
- 607 5. Langelier, M.-F., Planck, J.L., Roy, S. & Pascal, J.M. Structural basis for DNA
608 damage-dependent poly(ADP-ribosylation) by human PARP-1. *Science (New York,*
609 *N.Y.)* **336**, 728-732 (2012).
- 610 6. Leidecker, O. et al. Serine is a new target residue for endogenous ADP-ribosylation
611 on histones. *Nat Chem Biol* **12**, 998-1000 (2016).
- 612 7. Buch-Larsen, S.C. et al. Mapping Physiological ADP-Ribosylation Using Activated
613 Ion Electron Transfer Dissociation. *Cell Reports* **32**, 108176 (2020).
- 614 8. Gibbs-Seymour, I., Fontana, P., Rack, J.G.M. & Ahel, I. HPF1/C4orf27 Is a PARP-1-
615 Interacting Protein that Regulates PARP-1 ADP-Ribosylation Activity. *Molecular cell*
616 **62**, 432-442 (2016).
- 617 9. Suskiewicz, M.J. et al. HPF1 completes the PARP active site for DNA damage-
618 induced ADP-ribosylation. *Nature* (2020).
- 619 10. Palazzo, L. et al. Serine is the major residue for ADP-ribosylation upon DNA
620 damage. *Elife* **7**(2018).
- 621 11. Bonfiglio, J.J. et al. Serine ADP-Ribosylation Depends on HPF1. *Molecular cell* **65**,
622 932-940.e6 (2017).
- 623 12. Rudolph, J., Roberts, G., Muthurajan, U.M. & Luger, K. HPF1 and nucleosomes
624 mediate a dramatic switch in activity of PARP1 from polymerase to hydrolase. *Elife*
625 **10** (2021).
- 626 13. Sun, F.H. et al. HPF1 remodels the active site of PARP1 to enable the serine ADP-
627 ribosylation of histones. *Nat Commun* **12**, 1028 (2021).

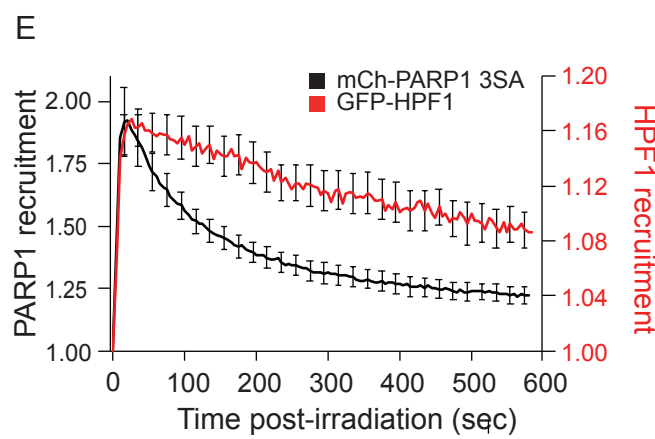
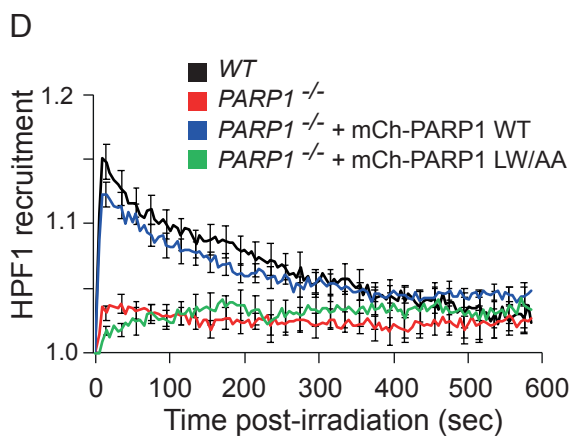
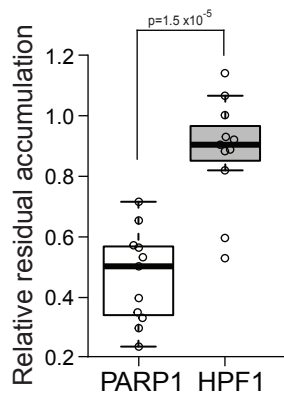
- 628 14. Mahadevan, J. et al. Q-FADD: A Mechanistic Approach for Modeling the
629 Accumulation of Proteins at Sites of DNA Damage. *Biophys J* **116**, 2224-2233
630 (2019).
- 631 15. Langelier, M.-F., Billur, R., Sverzhinsky, A., Black, B.E. & Pascal, J.M. HPF1
632 dynamically controls the PARP1/2 balance between initiating and elongating ADP-
633 ribose modifications. *bioRxiv*, 2021.05.19.444852 (2021).
- 634 16. Prokhorova, E. et al. Serine-linked PARP1 auto-modification controls PARP inhibitor
635 response. *Nature Communications* **12**, 4055 (2021).
- 636 17. Juhász, S. et al. The chromatin remodeler ALC1 underlies resistance to PARP
637 inhibitor treatment. *Science Advances* **6**, eabb8626 (2020).
- 638 18. Shao, Z. et al. Clinical PARP inhibitors do not abrogate PARP1 exchange at DNA
639 damage sites in vivo. *Nucleic Acids Research* **48**, 9694-9709 (2020).
- 640 19. Gibson, B.A., Conrad, L.B., Huang, D. & Kraus, W.L. Generation and
641 Characterization of Recombinant Antibody-like ADP-Ribose Binding Proteins.
642 *Biochemistry* **56**, 6305-6316 (2017).
- 643 20. Timinszky, G. et al. A macrodomain-containing histone rearranges chromatin upon
644 sensing PARP1 activation. *Nat Struct Mol Biol* **16**, 923-9 (2009).
- 645 21. Wang, Z. et al. Recognition of the iso-ADP-ribose moiety in poly(ADP-ribose) by
646 WWE domains suggests a general mechanism for poly(ADP-ribosyl)ation-dependent
647 ubiquitination. *Genes Dev* **26**, 235-40 (2012).
- 648 22. Smith, R. et al. Poly(ADP-ribose)-dependent chromatin unfolding facilitates the
649 association of DNA-binding proteins with DNA at sites of damage. *Nucleic Acids*
650 *Research* **47**, 11250-11267 (2019).
- 651 23. Sellou, H. et al. The poly(ADP-ribose)-dependent chromatin remodeler Alc1 induces
652 local chromatin relaxation upon DNA damage. *Molecular biology of the cell* **27**,
653 3791-3799 (2016).
- 654 24. Rother, M.B. et al. CHD7 and 53BP1 regulate distinct pathways for the re-ligation of
655 DNA double-strand breaks. *Nature Communications* **11**, 5775 (2020).
- 656 25. Smith, R., Sellou, H., Chapuis, C., Huet, S. & Timinszky, G. CHD3 and CHD4
657 recruitment and chromatin remodeling activity at DNA breaks is promoted by early
658 poly(ADP-ribose)-dependent chromatin relaxation. *Nucleic acids research* **46**, 6087-
659 6098 (2018).
- 660 26. Pfeiffer, A. et al. Poly(ADP-ribosyl)ation temporally confines SUMO-dependent
661 ataxin-3 recruitment to control DNA double-strand break repair. *J Cell Sci* **134**(2021).
- 662 27. Pan, M.R. et al. Chromodomain helicase DNA-binding protein 4 (CHD4) regulates
663 homologous recombination DNA repair, and its deficiency sensitizes cells to
664 poly(ADP-ribose) polymerase (PARP) inhibitor treatment. *J Biol Chem* **287**, 6764-72
665 (2012).
- 666 28. Liu, C., Vyas, A., Kassab, M.A., Singh, A.K. & Yu, X. The role of poly ADP-
667 ribosylation in the first wave of DNA damage response. *Nucleic Acids Res* **45**, 8129-
668 8141 (2017).
- 669 29. Barkauskaite, E., Jankevicius, G., Ladurner, A.G., Ahel, I. & Timinszky, G. The
670 recognition and removal of cellular poly(ADP-ribose) signals. *Febs j* **280**, 3491-507
671 (2013).
- 672 30. Murai, J. et al. Trapping of PARP1 and PARP2 by Clinical PARP Inhibitors. *Cancer*
673 *Res* **72**, 5588-99 (2012).
- 674 31. Poirier, G.G., de Murcia, G., Jongstra-Bilen, J., Niedergang, C. & Mandel, P.
675 Poly(ADP-ribosyl)ation of polynucleosomes causes relaxation of chromatin structure.
676 *Proc Natl Acad Sci U S A* **79**, 3423-7 (1982).
- 677 32. Hananya, N., Daley, S.K., Bagert, J.D. & Muir, T.W. Synthesis of ADP-Ribosylated
678 Histones Reveals Site-Specific Impacts on Chromatin Structure and Function. *Journal*
679 *of the American Chemical Society* **143**, 10847-10852 (2021).

- 680 33. de Murcia, G. et al. Modulation of chromatin superstructure induced by poly(ADP-
681 ribose) synthesis and degradation. *J Biol Chem* **261**, 7011-7 (1986).
- 682 34. Fontana, P. et al. Serine ADP-ribosylation reversal by the hydrolase ARH3. *Elife*
683 **6**(2017).
- 684 35. Hatakeyama, K., Nemoto, Y., Ueda, K. & Hayaishi, O. Purification and
685 characterization of poly(ADP-ribose) glycohydrolase. Different modes of action on
686 large and small poly(ADP-ribose). *J Biol Chem* **261**, 14902-11 (1986).
- 687 36. Luijsterburg, M.S. et al. PARP1 Links CHD2-Mediated Chromatin Expansion and
688 H3.3 Deposition to DNA Repair by Non-homologous End-Joining. *Mol Cell* **61**, 547-
689 562 (2016).
- 690 37. Bacic, L. et al. Structure and dynamics of the chromatin remodeler ALC1 bound to a
691 PARylated nucleosome. *bioRxiv*, 2021.06.18.448936 (2021).
- 692 38. Beaudouin, J., Mora-Bermúdez, F., Klee, T., Daigle, N. & Ellenberg, J. Dissecting the
693 Contribution of Diffusion and Interactions to the Mobility of Nuclear Proteins.
694 *Biophys J* **90**, 1878-94 (2006).
- 695 39. Polo, S.E., Kaidi, A., Baskcomb, L., Galanty, Y. & Jackson, S.P. Regulation of DNA-
696 damage responses and cell-cycle progression by the chromatin remodelling factor
697 CHD4. *Embo j* **29**, 3130-9 (2010).
- 698 40. Richardson, C., Moynahan, M.E. & Jasin, M. Double-strand break repair by
699 interchromosomal recombination: suppression of chromosomal translocations. *Genes*
700 *Dev* **12**, 3831-42 (1998).
- 701 41. Czarna, A. et al. Structures of Drosophila cryptochrome and mouse cryptochrome1
702 provide insight into circadian function. *Cell* **153**, 1394-405 (2013).
- 703 42. Gunn, A. & Stark, J.M. I-SceI-based assays to examine distinct repair outcomes of
704 mammalian chromosomal double strand breaks. *Methods Mol Biol* **920**, 379-91
705 (2012).
706

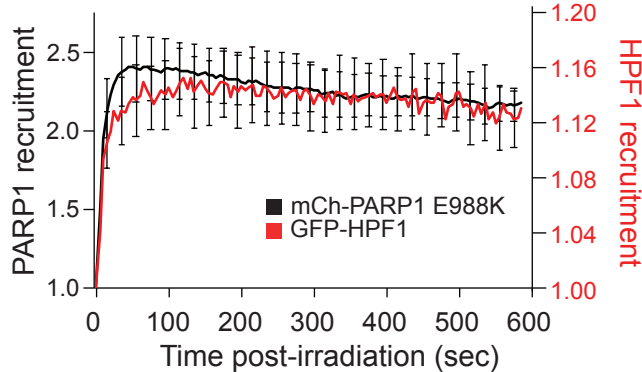
A



C



F



G

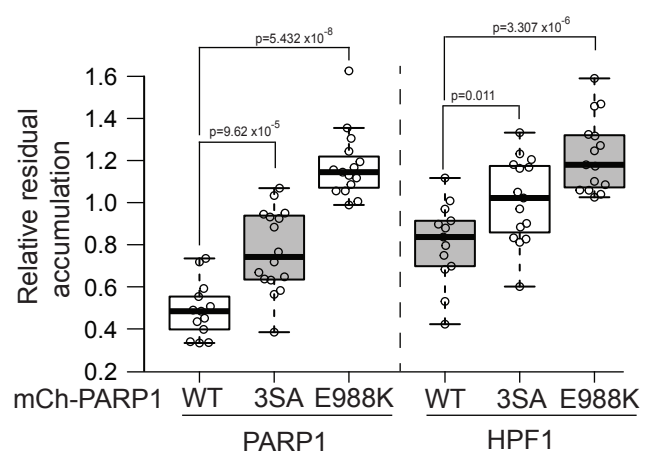


Figure 1: HPF1 recruitment to sites of damage relies on interaction with the C-terminus of PARP1. (A) Representative images of mCherry-PARP1 and GFP-HPF1 recruitment to sites of DNA damage induced by laser irradiation, in *PARP1*^{KO} cells. Scale bar, 5 μ m. (B) Recruitment kinetics of mCherry-PARP1 (black) and GFP-HPF1 (red) to sites of DNA damage. (C) To assess the relative release kinetics of mCherry-PARP1 and GFP-HPF1, the time $t_{1/2}$ at which half of PARP1-WT has been released compared to peak accumulation was first estimated from the mean curve shown in B. Then, the amount of the different proteins is measured at $t_{1/2}$ for each individual cell and normalized to peak accumulation to estimate the relative residual accumulation. (D) Recruitment kinetics of GFP-HPF1 to sites of DNA damage in *WT* or *PARP1*^{KO} cells expressing mCherry-tagged PARP1 WT or PARP1 L1013A/W1014A (PARP1-LW/AA). (E, F) Recruitment kinetics of (E) mCherry-PARP1-3SA (black) or (F) mCherry-PARP1-E988K (black) and GFP-HPF1 (red) to sites of DNA damage. (G) With the same approach as for panel C, the relative residual accumulation of mCherry tagged PARP1 mutants and GFP-HPF1 was estimated from the curves shown in E and F.

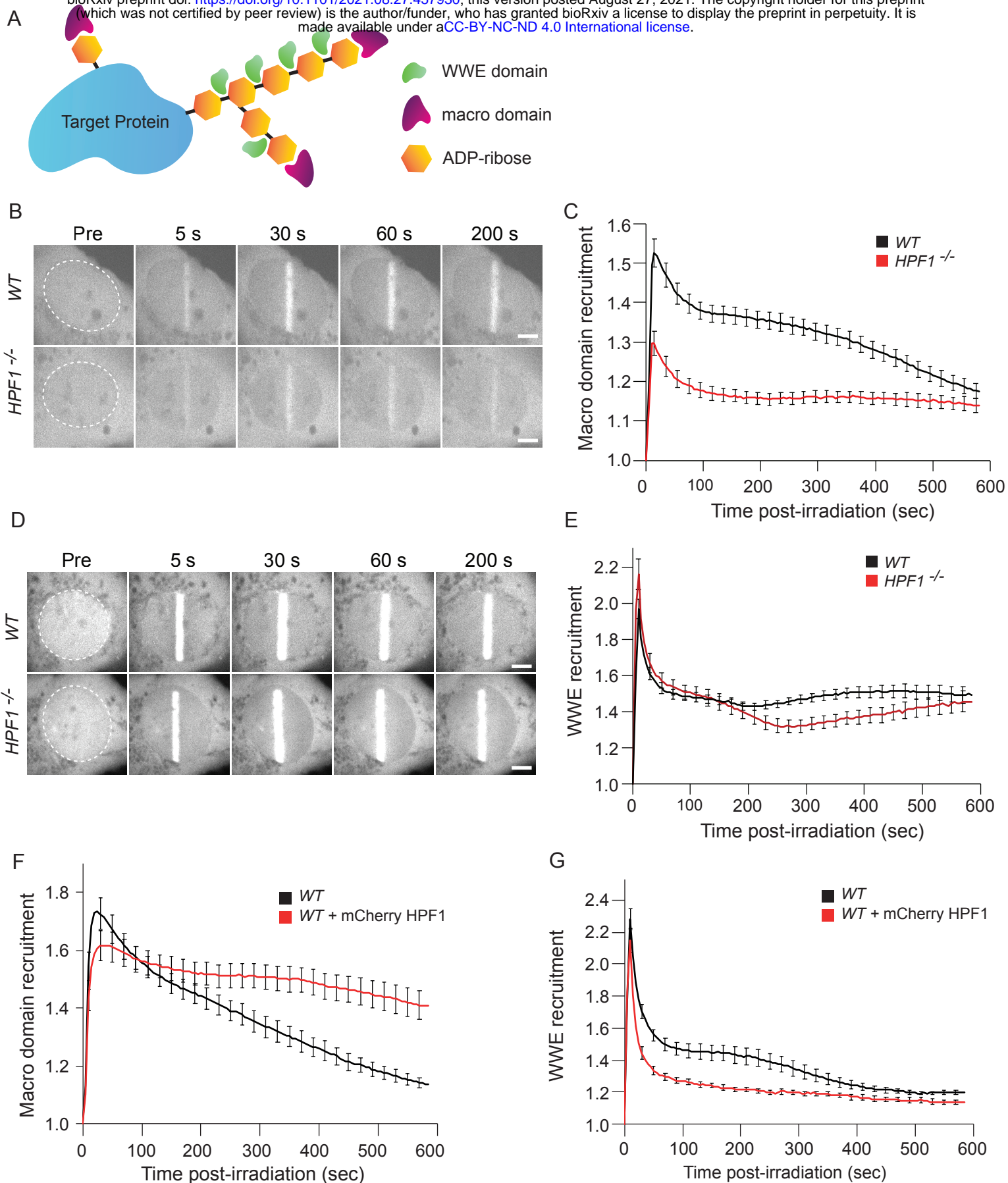


Figure 2: HPF1 regulates ADP-ribosylation signalling at sites of DNA damage. (A) Schematic representation of WWE and macrodomain recruitment on ADPr chains. (B) Representative images showing recruitment of the macrodomain of macroH2A1.1 to sites of DNA damage induced by laser irradiation in WT and *HPF1*^{KO} cells. Scale bar, 5 μm. (C) Recruitment kinetics of the macrodomain to sites of DNA damage in WT (black) and *HPF1*^{KO}(red) cells. (D) Representative images showing recruitment of the WWE domain of RNF146 to sites of laser induced DNA damage in WT and *HPF1*^{KO} cells. Scale bar, 5 μm. (E) Recruitment kinetics of the WWE domain to sites of DNA damage in WT (black) and *HPF1*^{KO}(red) cells. (F, G) Recruitment kinetics of (F) GFP-WWE or (G) GFP-macrodomain of mH2A1.1 recruitment kinetics at sites of DNA damage in U2OS WT cells overexpressing mCherry-HPF1 or not. Data are shown as mean ± SEM.

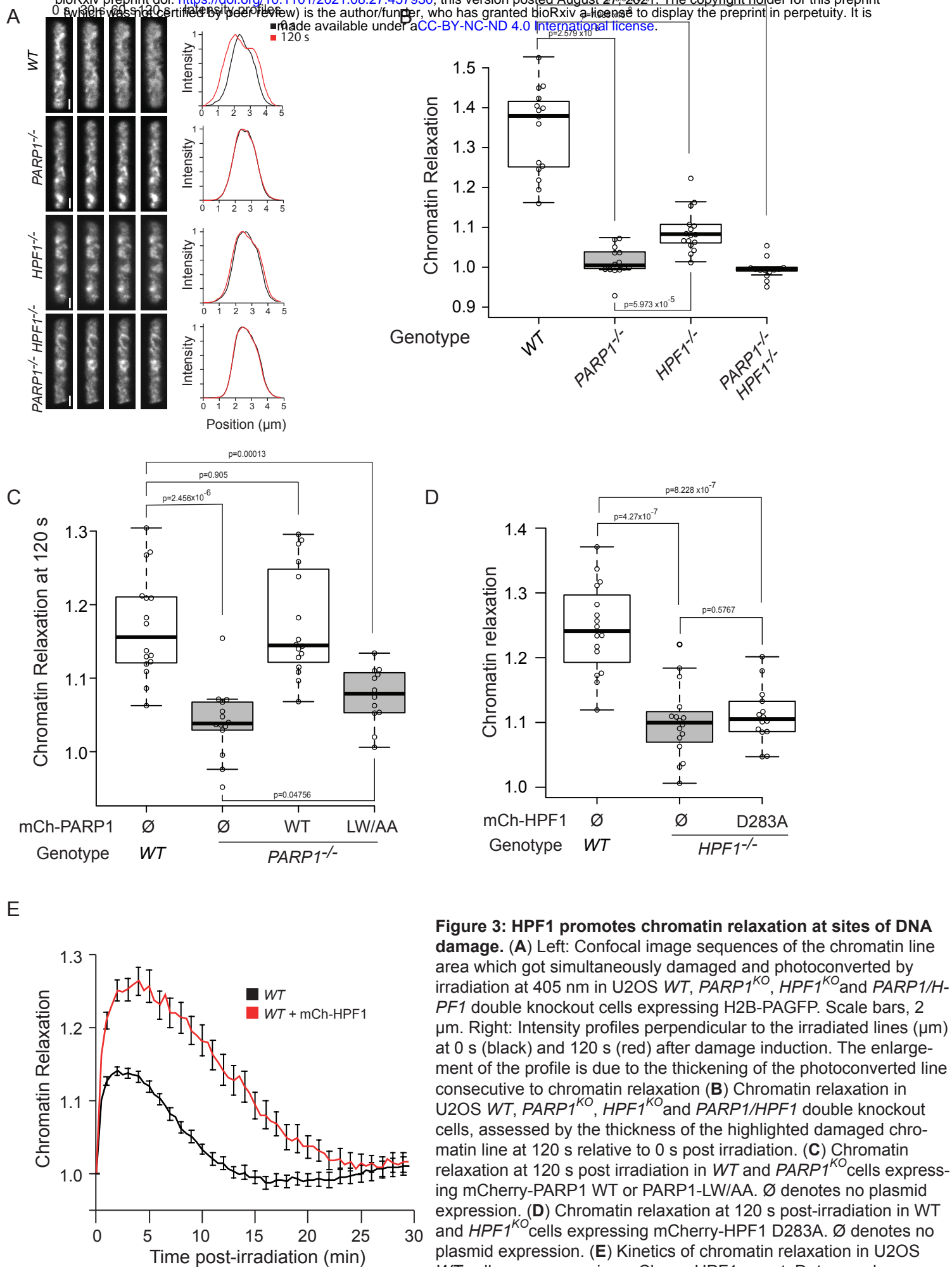
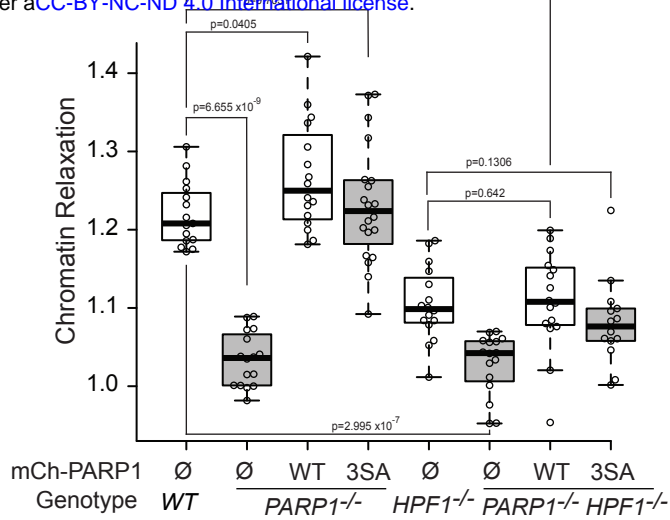
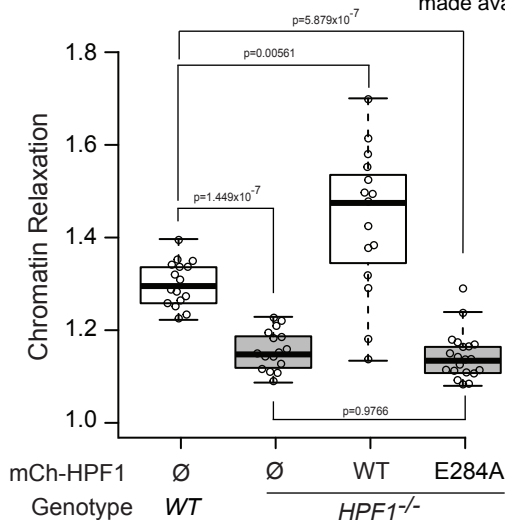
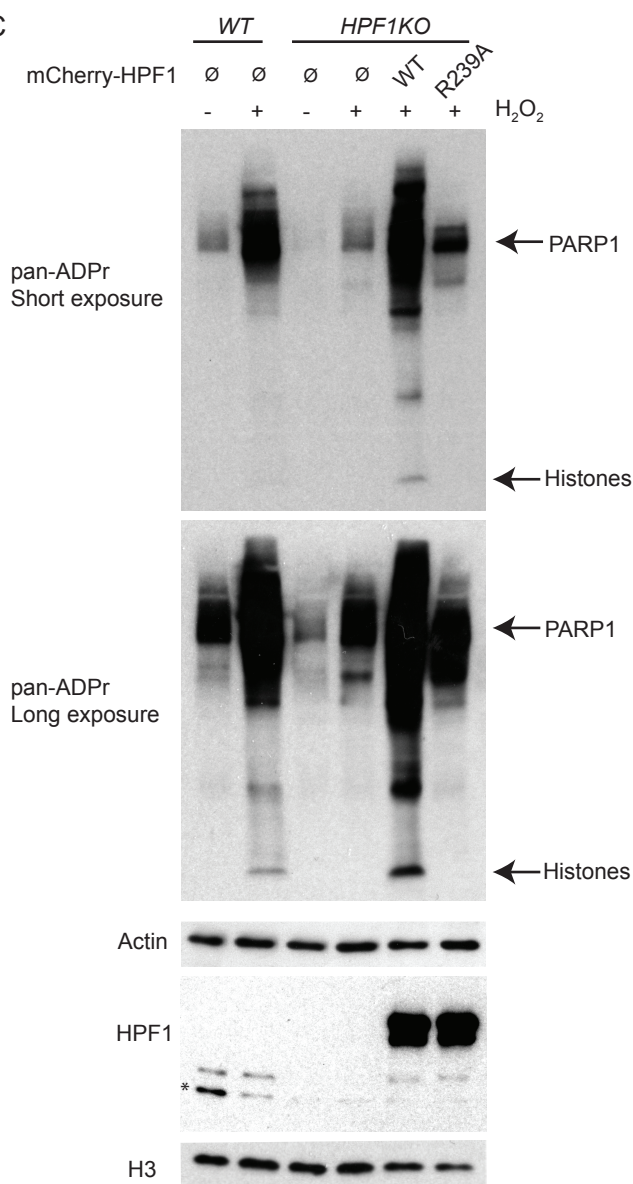


Figure 3: HPF1 promotes chromatin relaxation at sites of DNA damage. (A) Left: Confocal image sequences of the chromatin line area which got simultaneously damaged and photoconverted by irradiation at 405 nm in U2OS WT, $PARP1^{KO}$, $HPF1^{KO}$ and $PARP1/HPF1$ double knockout cells expressing H2B-PAGFP. Scale bars, 2 μ m. Right: Intensity profiles perpendicular to the irradiated lines (μ m) at 0 s (black) and 120 s (red) after damage induction. The enlargement of the profile is due to the thickening of the photoconverted line consecutive to chromatin relaxation (B) Chromatin relaxation in U2OS WT, $PARP1^{KO}$, $HPF1^{KO}$ and $PARP1/HPF1$ double knockout cells, assessed by the thickness of the highlighted damaged chromatin line at 120 s relative to 0 s post irradiation. (C) Chromatin relaxation at 120 s post irradiation in WT and $PARP1^{KO}$ cells expressing mCherry-PARP1 WT or PARP1-LW/AA. \emptyset denotes no plasmid expression. (D) Chromatin relaxation at 120 s post-irradiation in WT and $HPF1^{KO}$ cells expressing mCherry-HPF1 D283A. \emptyset denotes no plasmid expression. (E) Kinetics of chromatin relaxation in U2OS WT cells overexpressing mCherry-HPF1 or not. Data are shown as mean \pm SEM.

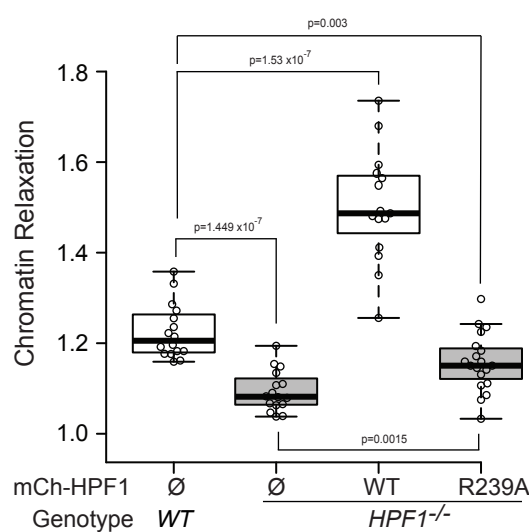
A



C



D



E

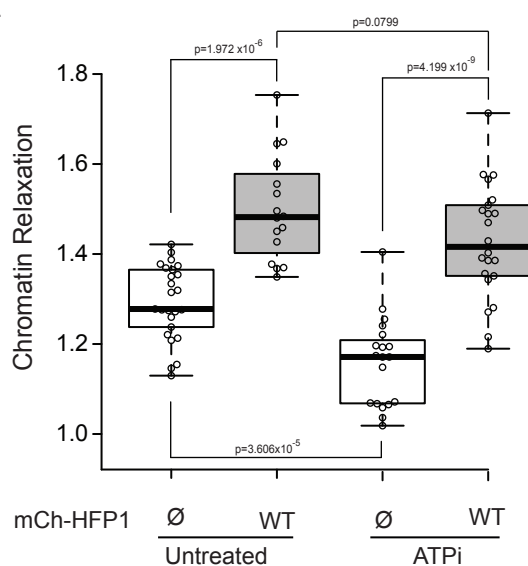


Figure 4: HPF1-dependent chromatin relaxation relies on trans ADP-ribosylation of histones rather than PARP1 auto-modification (A) Chromatin relaxation at 120 s post-irradiation in WT and *HPF1*^{KO} cells expressing or not mCherry-HPF1 E284A. ∅ denotes no plasmid expression. **(B)** Chromatin relaxation at 120s post-irradiation in U2OS WT, *PARP1*^{KO}, *HPF1*^{KO} and *PARP1/H-HPF1* double knockout cell. Cells are complemented either with mCherry-PARP1 WT or with PARP1-3SA mutant. ∅ denotes no plasmid expression. **(C)** Western blot displaying ADPr signals, stained with a pan-ADPr antibody, in WT and *HPF1*^{KO} cells expressing HPF1-WT or HPF1-R239A and treated or not with H₂O₂. H3 and Tubulin were used as loading controls. **(D)** Chromatin relaxation at 120 s post-irradiation in WT and *HPF1*^{KO} cells expressing mCherry-HPF1 R239A. ∅ denotes no plasmid expression. **(E)** Chromatin relaxation at 120 s post-irradiation in U2OS WT cells overexpressing mCherry-HPF1 and depleted or not for ATP (ATPi). ∅ denotes no plasmid expression.

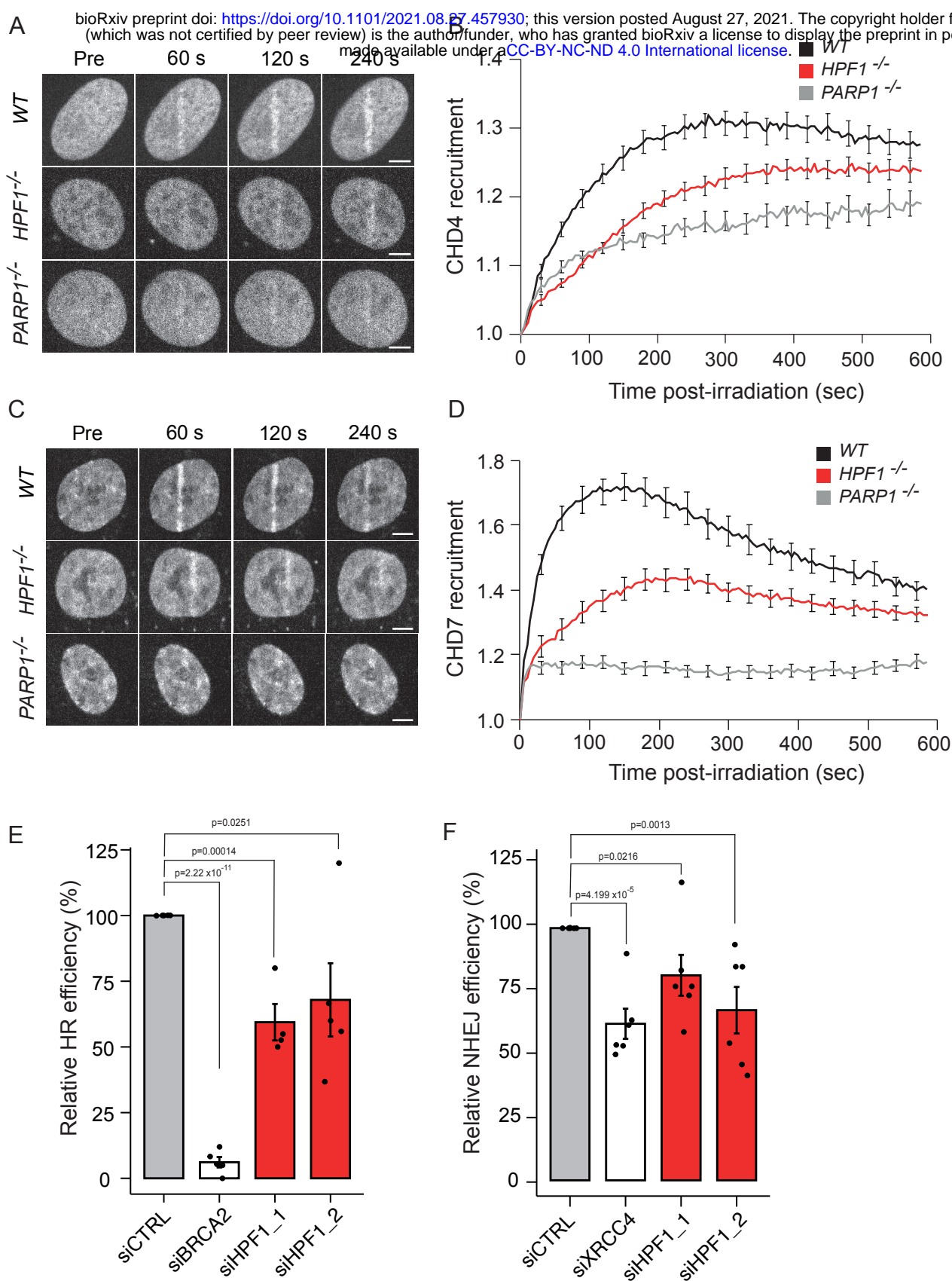


Figure 5: HPF1-dependent chromatin relaxation promotes the recruitment of both homologous recombination and non-homologous end joining repair factors. (A) Representative confocal images showing recruitment of GFP-CHD4 to sites DNA damage induced by laser irradiation, in U2OS WT, *HPF1*^{KO} or *PARP1*^{KO} cells. Scale bar, 5 μ m. (B) Recruitment kinetics of GFP-CHD4 to sites of DNA damage in U2OS WT, *HPF1*^{KO} or *PARP1*^{KO} cells. (C) Representative confocal images showing recruitment of GFP-CHD7 to sites of DNA damage induced by laser irradiation, in U2OS WT, *HPF1*^{KO} or *PARP1*^{KO} cells. Scale bar, 5 μ m. (D) Recruitment kinetics of GFP-CHD7 to sites of DNA damage in U2OS WT, *HPF1*^{KO} or *PARP1*^{KO} cells. (E) Quantification of DR-GFP-positive U2OS cells transfected with the indicated siRNA and I-SceI expression vector. The mean \pm SEM of 5 independent experiments is shown. Data were normalized to siCTRL, which was set to 100%. (F) Quantification of EJ5-GFP-positive U2OS cells transfected with the indicated siRNA and I-SceI expression vector. The mean \pm SEM of 6 independent experiments is shown. Data were normalized to siCTRL, which was set to 100%.

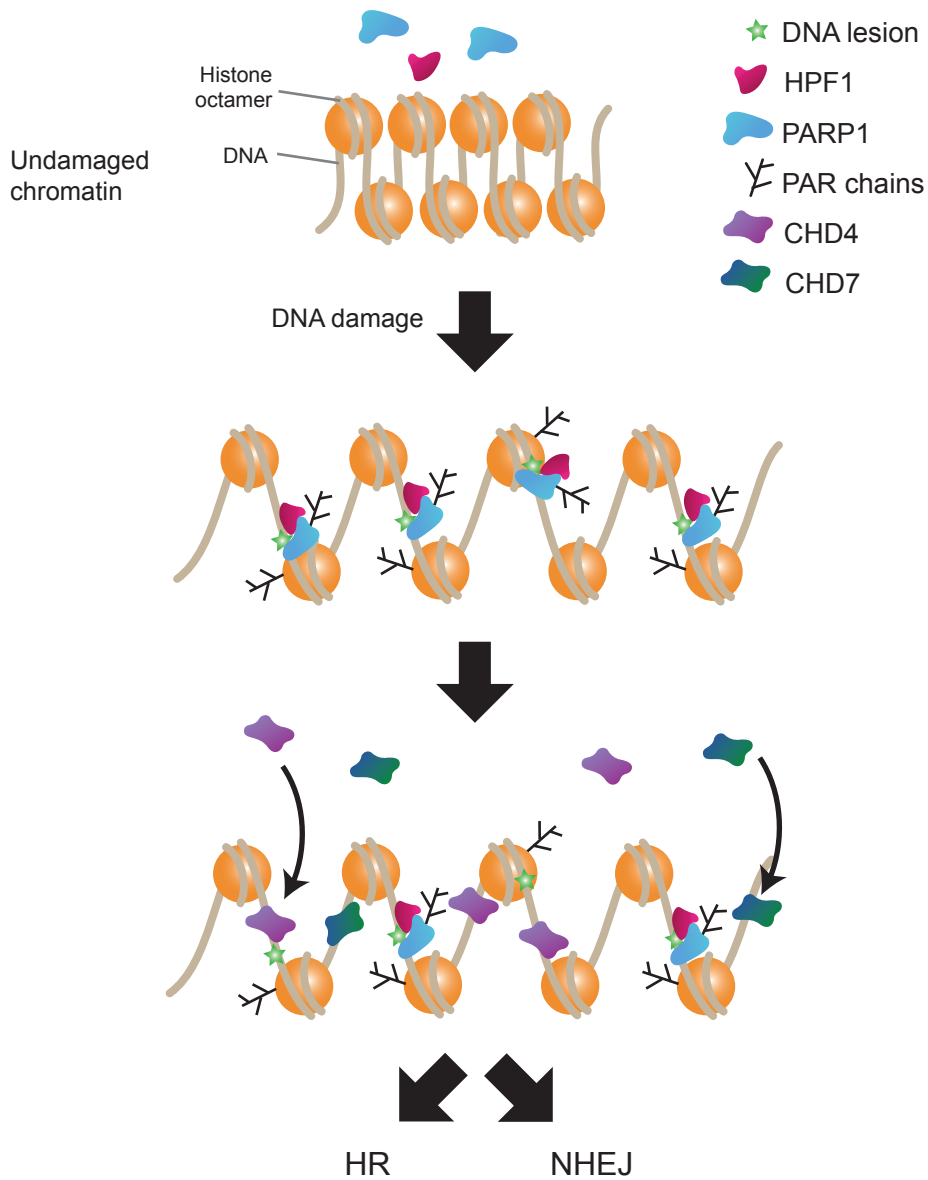
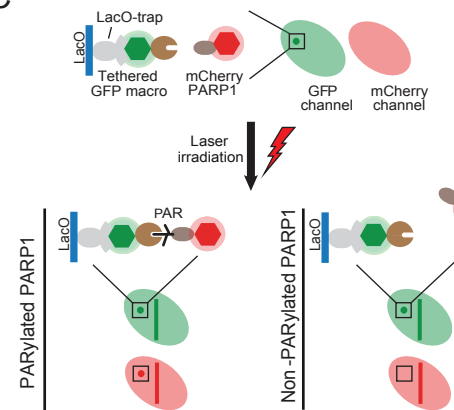
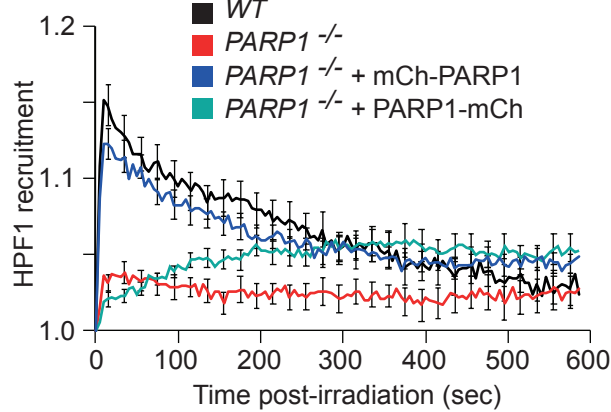
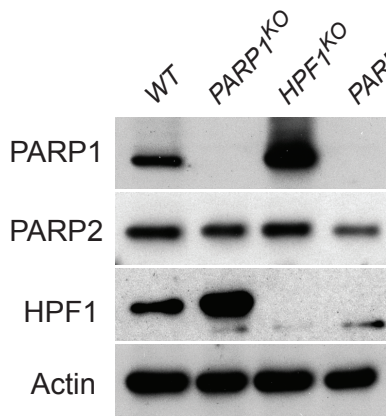
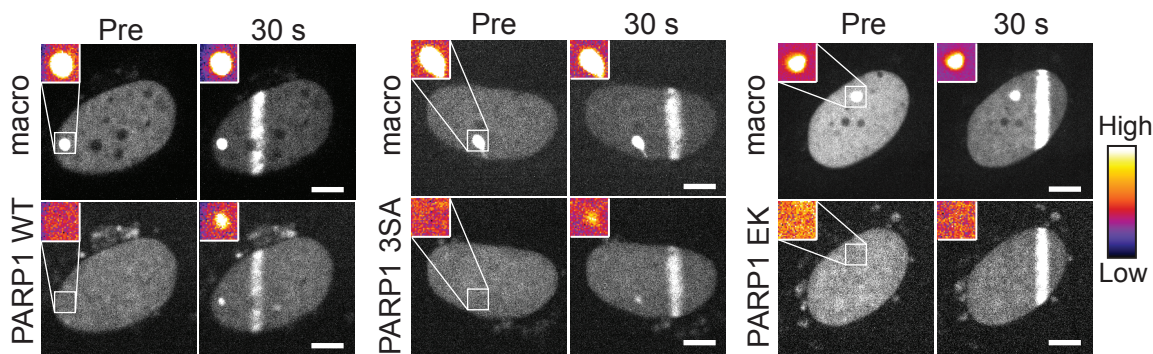


Figure 6: HPF1 regulates DNA damage induced chromatin relaxation. Upon damage, HPF1 interacts with PARP1 at sites of damage and promote both PARP1 auto-modification and trans ADP-ribosylation of histone. Histone ADP-ribosylation promotes chromatin relaxation in the vicinity of DNA lesions, promoting the recruitment of repair factors to facilitate genome restoration by both homologous recombination and non-homologous end joining.

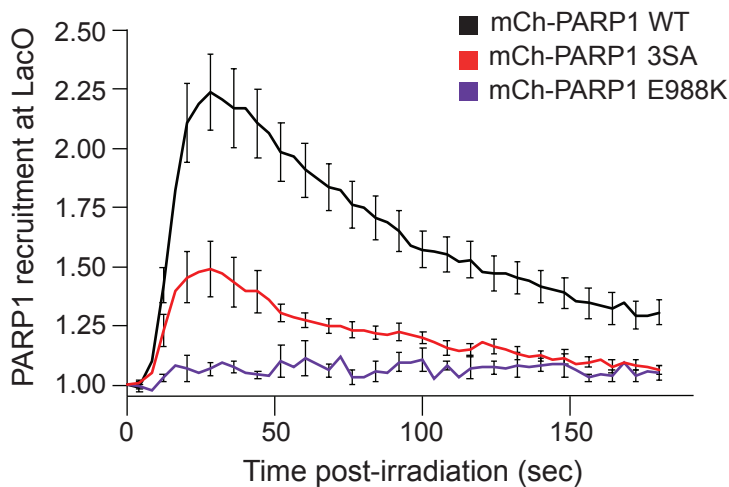
A



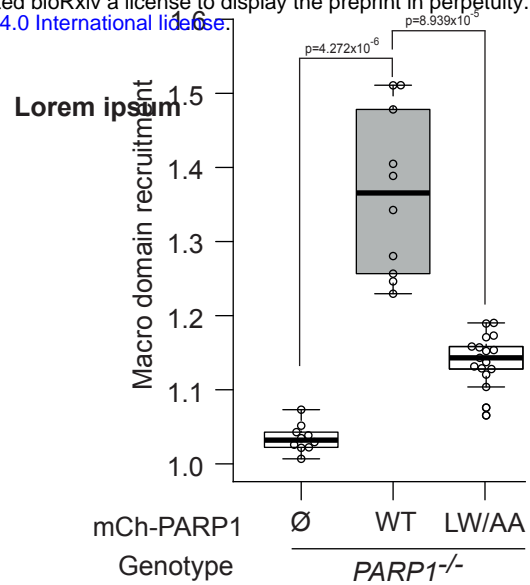
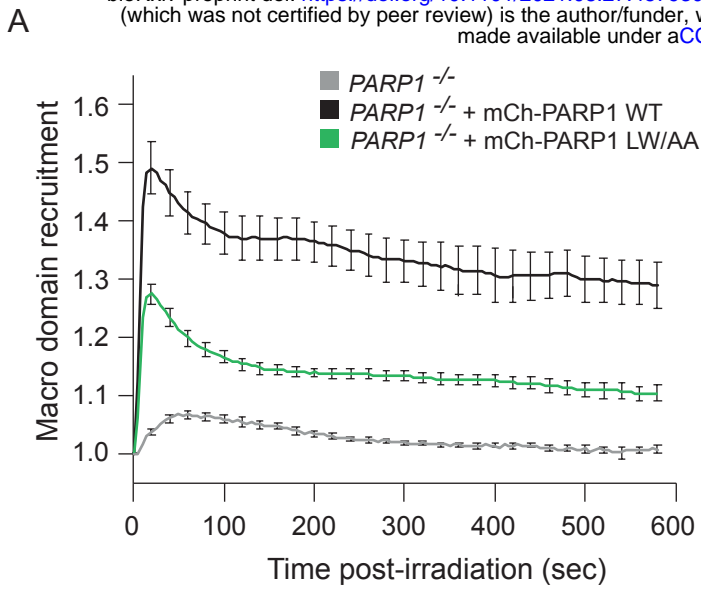
D



E



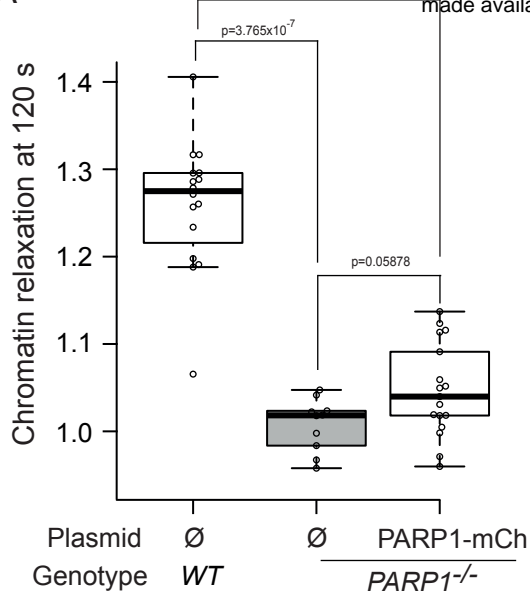
Supp Figure 1: HPF1 recruitment to sites of damage relies on interaction with the C-terminus of PARP1 (A) Immunoblots of whole cell extract from U2OS WT, *PARP1*^{KO}, *HPF1*^{KO} and *PARP1/HPF1* double knockout cells. Actin is used as a loading control. (B) Recruitment kinetics of GFP-HPF1 to sites of DNA damage in WT or *PARP1*^{KO} cells expressing WT N-terminally (mCh-PARP1) and C-terminally tagged PARP1 (PARP1-mCh). Data are shown as mean \pm SEM. (C) Schematic representation of PAR-3H assay. In this assay, mCherry-tagged PARP1 variants are expressed together with the GFP-tagged macrodomain of macroH2A1.1, that is tethered to a LacO array integrated into the genome of U2OS 2B2 cells. Upon laser irradiation, the PARP1 variants recruit to sites of damage, where they can be auto ADP-ribosylated or not, depending on the variant. A defect in auto ADP-ribosylation does not preclude high turnover at sites of damage, allowing all PARP1 variants to diffuse rapidly within the nucleus after their release from the DNA lesions. If PARP1 is ADP-ribosylated it can then interact with the tethered macrodomain leading to an increase in mCherry signal at the LacO array. (D) Representative confocal images of PARP1-WT, PARP1-3SA or PARP1-E988K to YFP-macrodomain of mH2A1.1 tethered to LacO. Inset, pseudocolored according to the look-up table displayed, shows the magnified LacO array. Post-irradiation images are shown at 30 seconds. Scale bar, 5 μ m. (E) Quantification of the accumulation of PARP1-WT, PARP1-3SA or PARP1-E988K to the LacO array after DNA induction by laser irradiation.



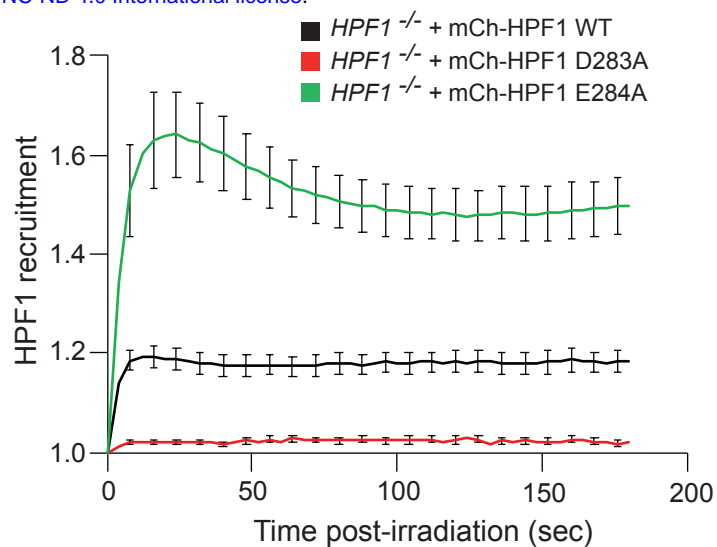
Supp Figure 2: HPF1 regulates ADP-ribosylation signalling at sites of DNA damage.

(A) Recruitment kinetics of GFP-macrodomain of mH2A1.1 at sites of DNA damage induced by laser irradiation, in U2OS *PARP1*^{KO} cells complemented or not with mCherry-PARP1 WT, PARP1-3SA or PARP1-LW/AA. (B) Quantification of mean intensity of GFP-macrodomain of mH2A1.1 at sites of DNA damage 200 s post-irradiation in *PARP1*^{KO} complemented or not with mCherry-PARP1 WT or PARP1-LW/AA mutants. Ø denotes no plasmid expression.

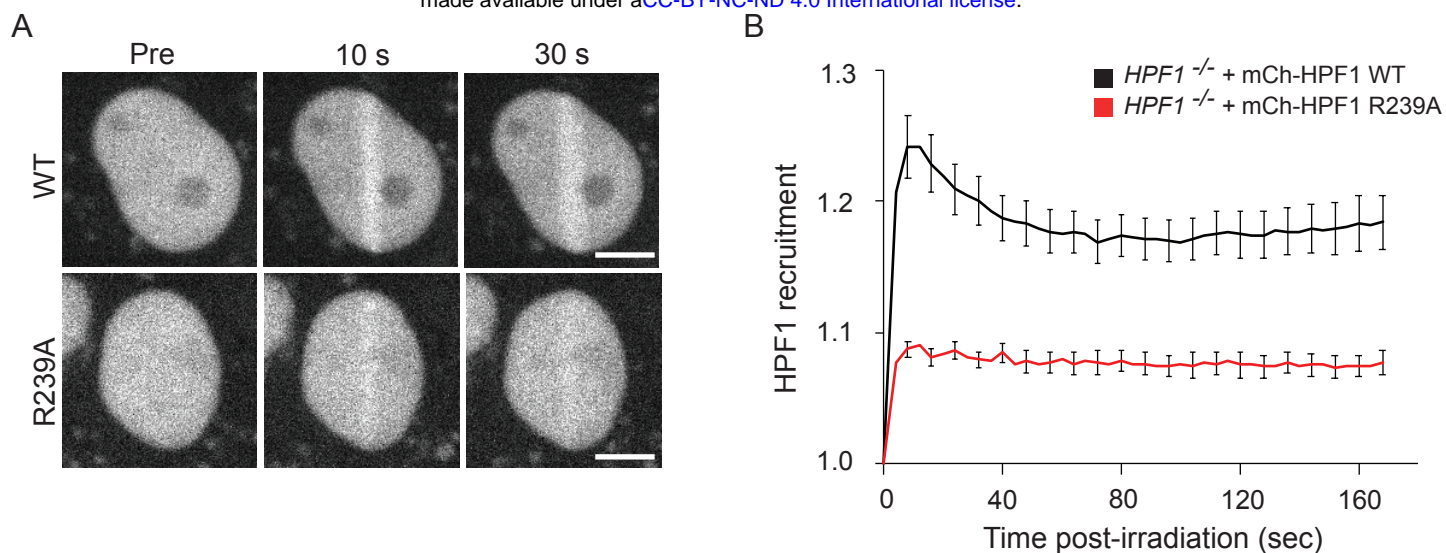
A



B

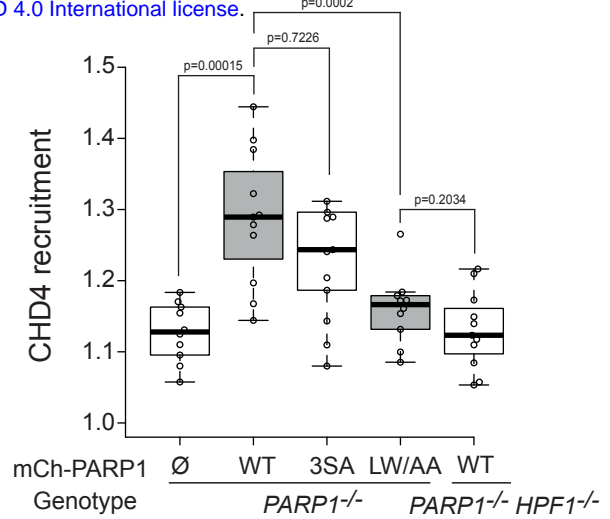
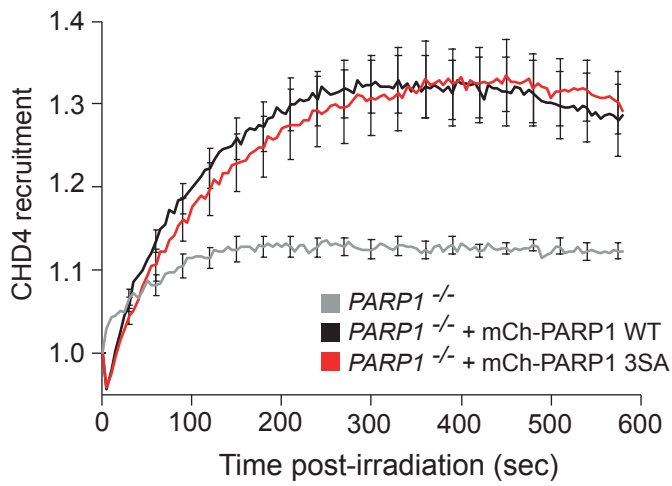


Supp Figure 3: HPF1 promotes chromatin relaxation at sites of DNA damage (A) Chromatin relaxation in U2OS *WT* or *PARP1*^{KO} cells at 120 s post-irradiation. Cells are complemented or not with C-terminally-tagged PARP1-mCherry. ∅ denotes no plasmid expression. **(B)** Recruitment kinetics of mCherry-tagged HPF1 WT and the point mutants D283A and E284A at sites of DNA damage in U2OS *HPF1*^{KO} cells.

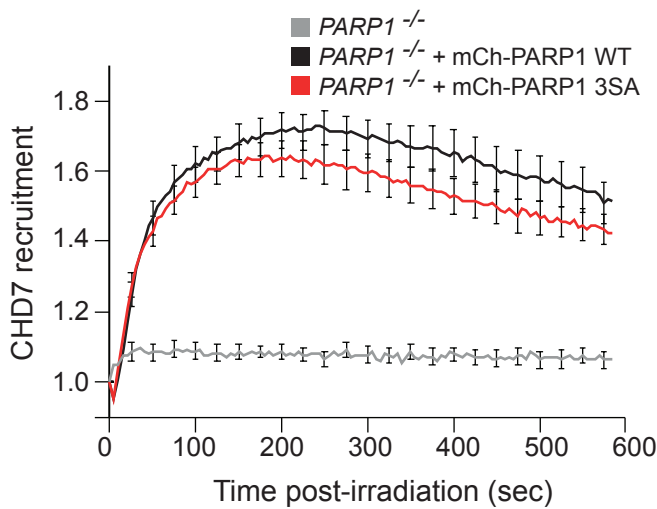


Supp Figure 4: HPF1-dependent chromatin relaxation relies on trans ADP-ribosylation of histones rather than PARP1 auto-modification (A) Representative images of the recruitment of mCherry-tagged HPF1 WT or HPF1-R239A to sites DNA damage induced by laser irradiation in U2OS *HPF1*^{KO} cells. Scale bar, 5 μ m. **(B)** Recruitment kinetics of mCherry-tagged HPF1 WT or HPF1-R239A mutant at sites of DNA damage in U2OS *HPF1*^{KO} cells.

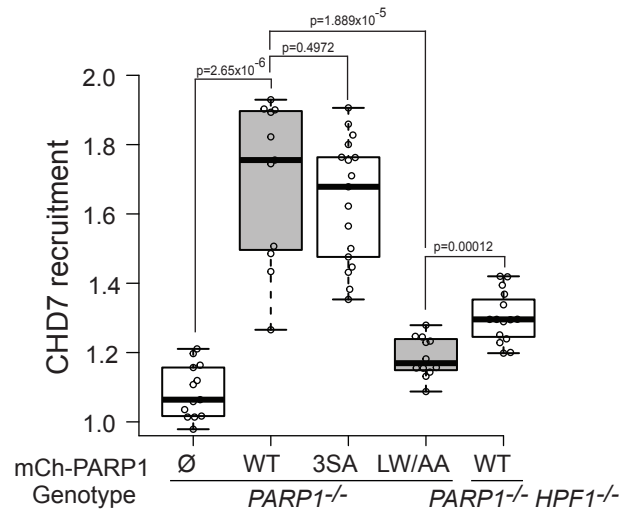
A



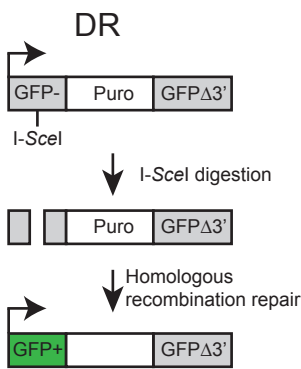
C



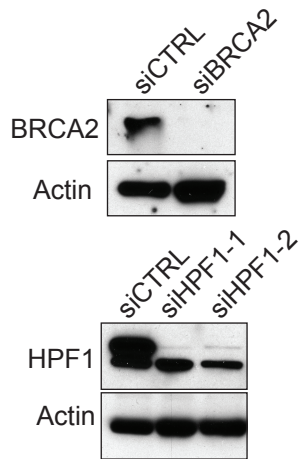
D



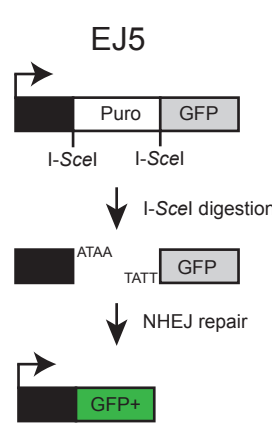
E



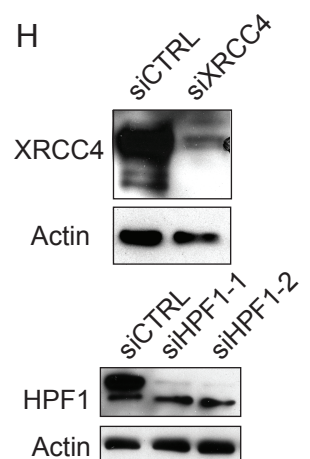
F



G



H



Supp Figure 5: HPF1 contributes to efficient repair by homologous recombination and non-homologous end joining.
(A) Recruitment kinetics of GFP-CHD4 to sites DNA damage in U2OS *WT*, *HPF1*^{KO} or *PARP1*^{KO} complemented or not with PARP1 WT or PARP1-3SA. **(B)** Quantification of mean intensity of GFP-CHD4 at sites DNA damage 200 s post-irradiation, in *PARP1*^{KO} or *PARP1/HPF1* double knockout cells complemented or not with mCherry-PARP1 WT, PARP-3SA or PARP1-LW/AA mutants. ∅ denotes no plasmid expression. **(C)** Recruitment kinetics of GFP-CHD7 to sites of DNA damage in U2OS *WT*, *HPF1*^{KO} or *PARP1*^{KO} complemented or not with PARP1 WT or PARP1-3SA. **(D)** Quantification of mean intensity of GFP-CHD7 at sites of DNA damage 200 s post-irradiation, in *PARP1*^{KO} or *PARP1/HPF1* double knockout cells complemented or not with mCherry-PARP1 WT, PARP-3SA or PARP1-LW/AA mutants. ∅ denotes no plasmid expression. **(E)** Schematic representation of the HR reporter assay (DR). After cleavage with I-SceI, the double-strand-breaks repaired by HR results in GFP expression. **(F)** Representative immunoblots showing the knockdown of BRCA2 and HPF1 in DR cells. Actin is used as a loading control. **(G)** Schematic representation of the NHEJ reporter assay (EJ5). Double cleavage by I-SceI removes the Puro cassette and the repair of the double-strand-break by NHEJ allows GFP expression. **(H)** Representative immunoblots showing knockdown of XRCC4 and HPF1 in EJ5 cells. Actin is used as a loading control.